Biomedicine & Pharmacotherapy 194 (2026) 118935

Contents lists available at ScienceDirect

Biomedicine & Pharmacotherapy

journal homepage: www.elsevier.com/locate/biopha

The binding of the salvianolic acid A to the citrullinating enzyme PADI4 as a potential treatment for cancer

Laureano E. Carpio [a,b,1], María Gabriela Álvarez-Rodríguez [c,1], David Recio-Moreno [c,d,1], Felipe Hornos [c], Izabel Georgieva-Nikolova [a], Ana Camara-Artigas [e], Virginia Rejas [f], Miguel Vidal [g], Martina Palomino-Schätzlein [a,b,*], Camino de Juan Romero [c,d,**], José L. Neira [c,h,***]

[a] Moldrug AI Systems SL, Olimpia Arozena Torres 45, Valencia 46018, Spain
[b] ProtoQSAR SL, Parque Tecnológico de Valencia, Nicolás Copérnico 6, Paterna, Valencia 46980, Spain
[c] IDIBE, Universidad Miguel Hernández, Elche, Alicante 03202, Spain
[d] Unidad de Investigación, Fundación para el Fomento de la Investigación Sanitaria y Biomédica de la Comunidad Valenciana (FISABIO), Hospital General Universitario de Elche, Camí de l'Almazara 11, Elche, Alicante 03203, Spain
[e] Departamento de Química y Física, Research Center CIAIMBITAL, Universidad de Almería-CeiA3, Almería 04120, Spain
[f] Centro de Investigación Príncipe Felipe, Calle de Eduardo Primo Yufera 3, Valencia 46013, Spain
[g] Centro de Investigaciones Biológicas Margarita Salas, CSIC, Calle Ramiro de Maeztu 9, Madrid 28040, Spain
[h] Institute of Biocomputation and Physics of Complex Systems (BIFI), Universidad de Zaragoza, Zaragoza 50018, Spain

ARTICLE INFO

Keywords:
Protein-drug interactions
Citrullinating enzyme
Proximity ligation assay
Molecular docking
NMR
Immunofluorescence

ABSTRACT

Cancer cells must maintain molecular mechanisms relying on an energy trade-off between resistance and key functions to survive. PADI4 (peptidyl arginine deiminase 4) is an enzyme implicated in the conversion of arginine to citrulline (citrullination), that has been related to the development of several types of cancers and in numerous inflammatory routes. Salvianolic acid A (SAA) is a stilbenoid, obtained from the radix of *Salvia miltiorrhiza*, with several anti-cancer and anti-inflammatory features. In this work, we report and characterize the interaction between PADI4 and SAA. The binding reaction was followed by using several biophysical probes, namely fluorescence, isothermal titration calorimetry (ITC) and nuclear magnetic resonance (NMR); the affinity constant was ~600 nM (ITC). The enzyme binding to the C-terminal region of RING1B (E3 ubiquitin-protein ligase really interesting new gene 1 B), which is a substrate of PADI4, was altered in the presence of SAA, as shown by NMR. Colorimetric assays indicated that SAA was an activator of the citrullinating activity of PADI4. Moreover, the results *in silico* suggested that binding of SAA to the dimeric PADI4 occurred at the dimerization interface, and not at its active site, potentially stabilizing the dimeric, active form of the protein. The effect of SAA was shown to be cell-line-dependent, and its presence in glioblastoma cells hampered the binding between intact RING1B

Abbreviations: BAEE, N-α-Benzoyl-L-arginine ethyl ester; COAD, colon cancer; COLDER, color developing reagent; C-RING1B, the C-terminal region residues 228–336 of RING1B; DMEM, Dulbecco's Modified Eagle's Medium; DMSO, di-methyl sulfoxide; DTT, dithiothreitol; EDTA, ethylenediaminetetraacetic acid; FBS, fetal bovine serum; GBM, glioblastoma; HSQC, heteronuclear single quantum coherence; GRP78, glucose regulated protein; ITC, isothermal titration calorimetry; LOGSY, ligand-observed via gradient spectroscopy; MD, molecular dynamics; MTT, 3–4,5-Dimethylthiazol-2-il-2,5-Diphenyl-2H-tetrazolium bromide; NET, neutrophil extracellular trap; NMR, nuclear magnetic resonance; PADI4, peptidyl arginine deiminase 4; PBS, phosphate buffered saline; PDAC, pancreatic ductal adenocarcinoma; PDB, Protein Data Bank; PFA, paraformaldehyde; PLA, proximity ligation assay; PTM, post-translational modification; RING, really interesting new gene; RING1B, E3 ubiquitin-protein ligase RING1; SAA, salvianolic acid A; RMSD, root mean square deviation; RMSF, root mean square fluctuation; ROS, reactive oxygen species; SASA, solvent accessible surface area; TCM, traditional Chinese medicine; TCEP, tris2-carboxyethylphosphine; TSC, thiosemicarbazide; TSP, trimethylsilylpropanoic acid; WaterLOGSSY, LOGSY occurring through transfer magnetization from the water.

* Corresponding author at: Moldrug AI Systems SL, Olimpia Arozena Torres 45, Valencia 46018, Spain.
** Corresponding author at: Unidad de Investigación, Fundación para el Fomento de la Investigación Sanitaria y Biomédica de la Comunidad Valenciana (FISABIO), Hospital General Universitario de Elche, Camí de l'Almazara 11, Elche, Alicante 03203, Spain.
*** Correspondence to: IDIBE, Edificio Torregaitán, Universidad Miguel Hernández, Avda. del Ferrocarril s/n, Elche, Alicante 03202, Spain.
E-mail addresses: mpalomino@protoqsar.com (M. Palomino-Schätzlein), m.juan@umh.es (C. de Juan Romero), jlneira@umh.es (J.L. Neira).
[1] These authors contributed equally to this work.

https://doi.org/10.1016/j.biopha.2025.118935
Received 25 September 2025; Received in revised form 14 December 2025; Accepted 17 December 2025
Available online 6 January 2026

and the enzyme. Altogether, this work shows that PADI4 was capable of binding to SAA, at a novel site, and opens the venue to develop its use in modulating *in vitro* and in cellular assays the deimination processes.

1. Introduction

Cancer remains one of the leading causes of morbidity and mortality worldwide, with approximately 20 million new cases of cancer being diagnosed in 2022 and nearly 10 million cancer-related deaths reported globally [1]. Conventional therapeutic strategies for cancer treatment include surgery, chemotherapy, and radiotherapy. However, challenges such as resistance, tumor recurrence, and metastasis continue to hinder long-term success and contribute to those high mortality rates (see, for instance [2]).

In recent years, Traditional Chinese Medicine (TCM) has attracted increased attention as a complementary or alternative therapy to conventional cancer treatments [3]. Clinical and preclinical studies have demonstrated the efficacy of compounds from TCM in alleviating cancer-related symptoms, enhancing patient quality of life, and potentially improving therapeutic outcomes when incorporated into multimodal treatment regimens [3]. Among the bioactive compounds derived from Chinese medicinal herbs, polyphenols are of interest due to their medical properties and minimal toxicity [4]. Polyphenols are a broad family of natural products encompassing phenolic acids, flavonoids, tannins and stilbenoids [5]; all of them are abundantly found in medicinal herbs and plants [6]. Polyphenols are the subject of extensive scientific interest because of their possible worthwhile effects on human health [7]. Salvianolic acid A (SAA) is a stilbenoid (Scheme 1), which is isolated from the radix of *Salvia miltiorrhiza*, as well as from the root extract of *Salvia yunnanensis*. Salvianolic acid A is a water-soluble compound with anti-inflammatory [8], anti-cancer [9] and anti-oxidant [10] properties. Furthermore, the roots of *Salvia miltiorrhiza* are utilized in TCM as a treatment for cancer [11].

PADI4 is a member of the family of peptidyl-arginine deiminases implicated in the process known as citrullination: the conversion of arginine to citrulline residues in a protein, when Ca^{2+} is present. This post-translational modification (PTM) is permanent, and it alters the molecular properties of the polypeptide chain, having important roles in human diseases [12–15]. Among other places, PADI4 is usually located in the cytoplasmic granules of eosinophils, neutrophils or macrophages, and in tumor cells, where PADI4 is highly expressed, either in the cytosol or in the nucleus, as we have shown in glioblastoma (GBM), pancreatic adenocarcinoma (PDAC) and colon cancer (COAD) [16]. PADI4 is also involved in gene transcription and immune system modulation [17–21]. An increase in its enzymatic activity is observed for several PADI4 haplotype mutants during apoptosis enhanced through the mitochondrial pathway [22], and such activation has also been detected in the presence of designed peptides [23]. PADI4 also regulates *p53* gene expression, as well as the expression of other *p53*-target genes [24–26]. We have recently shown that PADI4 binds to other key proteins involved in several cell processes and cancer development, such as importin α3 [27]; plakophilin 1 (PKP1) [28]; murine double minute 2 (MDM2) and fragments from it [29,30]; the nuclear protein 1 (NUPR1) [31]; the RING and YY1-binding protein (RYBP) [32]; and the Really Interesting New Gene protein 1B (RING1B), whose C-terminal region (residues 228–336 of the intact protein, C-RING1B) is a substrate of PADI4 [33]. We have also shown that PADI4 is capable of binding to lipids [34].

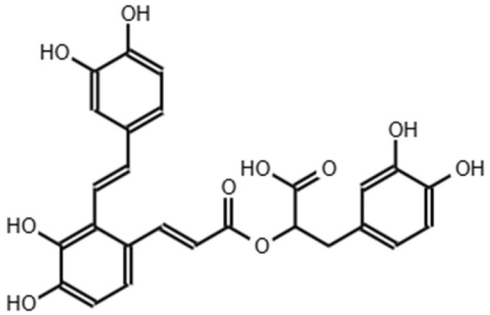

Scheme 1. Structure of Salvianolic acid A.

In this work, we investigated the binding between PADI4 and SAA *in vitro*, in cellular assays and *in silico*. We obtained an affinity constant of ~0.6 μM, as shown by fluorescence and isothermal titration calorimetry (ITC). The binding between PADI4 and C-RING1B, as shown by 2D ^{1}H-^{15}N HSQC NMR, was modified by the presence of SAA. However, the SAA acted as an activator of the enzymatic activity of the protein, as shown by colorimetric (COLDER) assays, suggesting that SAA was bound to an allosteric site of the protein. This was confirmed by molecular docking studies, where the most favorable binding pose of the stilbenoid was detected at the interface of the PADI4 dimer and not at its active site. We also showed that in the presence of SAA, the binding between the intact RING1B and PADI4 was abolished in GBM cells; assays with different cell lines also showed that cellular proliferation was affected by the presence of the stilbenoid and it was cell-dependent. Then, we can conclude that SAA was bound to PADI4, opening the possibility of using this natural product as an agent to modulate the enzymatic activity of PADI4.

2. Materials and methods

2.1. Materials

Imidazole, Trizma base and acid, DNase, glycerol, N-α-Benzoyl-L-arginine ethyl ester (BAEE), L-citrulline, 3-hydroxyimino 2-butanone (diacetyl monoxime), thiosemicarbazide (TSC), SO_4H_2 (98 %), PO_4H_3 (85 %), $NH_4Fe(SO_4)_2 \times 12\ H_2O$, NaCl, antipyrine, 3-(4,5-Dimethylthiazol-2-il)-2,5-Diphenyl-2H-tetrazolium bromide (MTT), SIGMAFAST protease tablets, NaCl, Ni^{2+}-resin, DAPI (4′,6-diamidino-2-phenylindole), dithiothreitol (DTT), trimethylsilylpropanoic acid (TSP), ethylenediaminetetraacetic acid (EDTA), di-methyl sulfoxide (DMSO), paraformaldehyde (PFA) and ultra-pure dioxane were from Sigma (Madrid, Spain). Kanamycin and isopropyl-β-D-1-thiogalactopyranoside were obtained from Apollo Scientific (Stockport, UK). Dialysis tubing with a molecular weight cut-off of 3500 Da, Triton X-100, TCEP (tris(2-carboxyethyl)phosphine) and the SDS protein marker (PAGEmark Tricolor), GSK484 (Cayman Chemical) were from VWR (Barcelona, Spain). SAA was purchased from Eurodiagnostico SL (Madrid, Spain). Amicon centrifugal devices with a molecular weight cut-off of 30 kDa were from Millipore (Barcelona, Spain).

The rest of the materials was of analytical grade. Water was deionized and purified on a Millipore system.

2.2. Protein expression and purification

The dimeric protein PADI4 (with 663 residues *per* monomer) was purified as previously described [16]. Protein concentration was determined by UV absorbance, employing an extinction coefficient at 280 nm estimated from the 10 tryptophans and 13 tyrosines *per* monomer [35].

The dimeric ^{15}N-labelled C-RING1B, at the C-terminal region of RING1B that comprises residues 228–336, is a substrate of PADI4 and binds to PADI4 in the low micromolar range [33]. The C-RING1B was purified as described [36]; its concentration was determined as that of PADI4 [35].

2.3. Binding experiments of SAA to PADI4 followed by fluorescence

We used SAA as a drug targeting PADI4 because of its long-term use in TCM, its anti-cancer properties and due to cost-effective reasons, namely, its commercial availability at affordable prices [9,11].

A Cary Varian spectrofluorometer (Agilent, Santa Clara, CA, USA), interfaced with a Peltier unit, was used to collect fluorescence spectra during the titration experiments, and thermal denaturations. For the steady-state experiments, the concentration of PADI4 was 2 μM (in protomer units) and that of SAA was 30 μM. Samples were excited at 280 or 295 nm, and the spectra were collected between 300 and 400 nm. The bandwidth was 1 nm; the slit widths for excitation and emission were 5 nm. The fluorescence experiments were carried out at 25 °C in buffer Tris 20 mM (pH 7.6), glycerol 10 % (vol/vol), 1 mM EDTA, TCEP 0.5 mM and 150 mM NaCl.

2.3.1. Titration experiments

For the titration between SAA and PADI4, increasing amounts of SAA, in the concentration range 0–30 μM, were added to a solution with a fixed concentration of PADI4 (2.0 μM in protomer units). The samples were prepared the day before and left overnight at 5 ºC; before the measurements, they were incubated for 1 h at 25 ºC. Experiments were carried out in the same buffer used for the steady-state experiments. The samples were excited at 280 and 295 nm, with a bandwidth of 1 nm; the slit widths were 5 nm for all experiments. In all cases, the appropriate blank-corrections were made by subtracting the signal obtained with the corresponding amounts of SAA by using KaleidaGraph (Synergy software, Reading, PA, USA). Spectra were corrected for inner-filter effects during fluorescence excitation [37]. The titration was repeated twice, using new samples; variations in the results of the two titrations were lower than 10 %.

The dissociation constant of the PADI4/SAA complex, K_d, was calculated by fitting the binding isotherm constructed by plotting the observed fluorescence change as a function of SAA concentration to the general binding model, explicitly taking into account protein depletion due to binding [38,39]:

$$F = F_0 + \frac{\Delta F_{max}}{2[PADI4]_T}\left(([SAA]_T + [PADI4]_T + K_d) - \sqrt{(([SAA]_T + [PADI4]_T + K_d)^2 - 4[SAA]_T[PADI4]_T}\right) \quad (1),$$

where F is the measured fluorescence at any particular concentration of SAA after subtraction of the spectrum of a sample containing only the same concentration of SAA (i.e., F is the difference fluorescence); ΔF_{max} is the largest change in the fluorescence of SAA when all polypeptide molecules were forming the complex, compared to the fluorescence of isolated enzyme (at the same corresponding concentration); F_0 is the fluorescence intensity when no SAA was added; $[PADI4]_T$ is the constant, total concentration of PADI4 (2.0 μM in protomer units); and $[SAA]_T$ is that of SAA, which was varied during the titration. Fitting to Eq. (1) was carried out by using KaleidaGraph.

We also carried out similar titrations with C-RING1B (at a concentration of 4 μM of protomer) and SAA, to elucidate whether binding of SAA to the domain also occurred.

2.3.2. Thermal denaturations

Thermal denaturation experiments were carried out by excitation at 280 and 295 nm, and following emission fluorescence at different wavelengths. The temperature range was measured from 25 to 85 ºC, with a step resolution of 0.2 ºC, an average time of 1 s and a scan speed of 1 ºC/min. Thermal scans were collected at 315, 330 and 350 nm after excitation at either 280 or 295 nm. The average time was 1 s, and the excitation and emission slits were set to 5 nm. Experiments were carried out with a sample with isolated PADI4 (at a concentration of 2 μM in protomer units) and another one with a concentration of SAA of 30 μM, at the same PADI4 concentration. The resulting thermograms were fitted to a two-state equation from where a thermal denaturation midpoint, T_m, was obtained to allow for an estimate of the conformational stability of PADI4 in the presence or in the absence of SAA [40]

2.4. Isothermal titration calorimetry (ITC)

The interaction of PADI4 with SAA was evaluated with a VP-ITC instrument (MicroCal, Northampton, USA). The ITC experiments were carried out at 25 °C in buffer Tris 20 mM (pH 7.6), glycerol 10 % (vol/vol), 1 mM EDTA, TCEP 0.5 mM and 150 mM NaCl.

These ITC experiments were carried out with twenty-nine 10-μL injections of ligand (with a total concentration of 120 μM of SAA in the syringe) into the calorimetric cell, that was filled with protein solution (3 μM PADI4 in protomer units). The injections were carried out with a reference power of 15μ Cal/s and a stirring speed of 307 rpm.

To correct for the dilution heat, generated by the dilution of the ligand solution into the calorimetric cell, an assay was performed in which the same concentration of ligand was injected over the buffer (within the calorimetric cell). Correction and fitting were obtained with these values, by using the manufacturer's software.

2.5. Nuclear Magnetic Resonance (NMR)

All the NMR spectra were acquired on a Bruker Avance 500 MHz spectrometer (Bruker GmbH, Germany), equipped with a triple resonance probe and z-pulse field gradients. Spectra were processed with Bruker TopSpin 2.1 (Bruker GmbH, Karlsruhe, Germany). The temperature of the probe was calibrated with pure methanol [41]. Spectra were calibrated with TSP, used as the internal chemical shift reference, and for the indirect ^{15}N dimension by considering the pH-dependent changes of its chemical shifts [41]. Unless it is indicated, all spectra were acquired at 20 ºC in 20 mM Tris buffer (pH 7.5), 5 mM TCEP, 150 mM NaCl, 10 mM EDTA, and 10 % glycerol with 50 μL of D_2O.

2.5.1. WaterLOGSY

The WaterLOGSY experiment transfers the large bulk water magnetization *via* the protein-ligand complex to the free ligand in a selective manner. In this experiment, the resonances of non-binding compounds appear with opposite sign to those of binders, and tend to be weaker than those belonging to the interacting ligands. This experiment can be used to select compounds from a large library capable of binding to a target, but in our case, we employed the technique to test whether SAA was bound to PADI4. Experiments were carried out in the above buffer at 25 ºC, in the presence of 10 μM of PADI4 (in protomer units) with an excess of SAA (140 μM), by using standard parameters for the length and the power of gradients found in the literature [42–44], namely, the relaxation and mixing times were 2.5 and 100 ms, respectively. The spectra were recorded with 256 scans and 32 K data points. The experiment was repeated twice with newly prepared samples. We also carried out control experiments with no PADI4 added to the solution containing only SAA, in the same buffer.

1D ^1H NMR spectra with each sample were also acquired to check for solutions stability by using the WATERGATE sequence [45].

2.5.2. 2D ^1H-^{15}N HSQC

Three different 2D 1H-15N HSQC NMR spectra [46] were obtained on samples containing: (i) isolated C-RING1B (90 μM of final concentration in protomer units); (ii) C-RING1B (90 μM of final concentration in protomer units) in the presence of 300 μM of PADI4 (final concentration in protomer units); and (iii) C-RING1B (90 μM of final concentration in protomer units) in the presence of 300 μM of PADI4 (final concentration in protomer units) and 300 μM of SAA; in all cases, the pH of the samples was pH 7.5. The pH of the three samples (complex PADI4/C-RING1B without SAA; complex PADI4/C-RING1B with SAA; and isolated C-RING1B) was measured after removal from the Amicon

device with an ultra-thin electrode before and after the acquisition of NMR spectra; the values of the pH reported here represent apparent values of pH, without correction for isotope effects. All spectra were acquired in the TPPI mode with 2048 complex points in the ^{1}H dimension, 200 complex points in the ^{15}N dimension, with 192 scans. The spectral widths for the 2D 1H-15N HSQC spectra were 6000 (^{1}H) and 1500 (^{15}N) Hz. Water was removed by using the WATERGATE sequence [45]. Experiments were carried out at 25 ºC.

The samples containing the mixture of PADI4 and C-RING1B (either in the presence or in the absence of SAA) were prepared by using Amicon centrifugal devices of 3 kDa cut-off, in which both proteins were initially mixed at diluted concentrations in the above indicated buffer, and then, concentrated in the same buffer; any possible precipitation product observed in the Amicon device was removed during the concentration step. For the experiments in the presence of SAA, after the concentration step, as described above, a corresponding volume of a concentrated stock solution of the stilbenoid (7 mM) was added to the solution of the complex. In both cases (either in the presence or absence of SAA), at the end of the concentration step, when the final volume of the concentrated solution was ~400 μL, 50 μL of D_2O and 50 μL of a concentrated (10 ×) stock solution of the above indicated fluorescence buffer were added. It is important to stress that no assignment of C-RING1B is available in the Biological Magnetic Resonance, and therefore, the HSQC spectra were used as qualitative indicators of changes occurring upon addition of PADI4, either in the presence or in the absence of SAA.

2.6. Far ultraviolet circular dichroism (far-UV CD)

Far-UV CD spectra were collected on a Jasco J810 spectropolarimeter (Jasco, Tokyo, Japan) with a thermostated cell holder and interfaced with a Peltier unit. The instrument was periodically calibrated with (+)-10-camphorsulfonic acid. A 0.1-cm path length quartz cell was used (Hellma, Kruibeke, Belgium). All spectra were corrected by subtracting the corresponding baseline. Concentration of PADI4 was 2 μM (in protomer units) and that of SAA was 30 μM; buffers were the same used for fluorescence experiments. Samples were prepared the day before and left overnight at 5 ºC to allow them to equilibrate. Before starting the experiments, samples were further left for 1 h at 25 ºC. SAA did not show any far-UV CD spectra; isothermal spectra of isolated PADI4 and that of the complex were acquired as an average of 6 scans, at a scan speed of 50 nm/min, with a response time of 2 s and a band-width of 1 nm, at 25 ºC.

2.7. Citrulline determination by a colorimetric assay

A photometric method used in the determination of L-citrulline was carried out to determine whether PADI4 was capable of citrullinating the BAEE in the presence of SAA. This method is based in the reaction of citrulline with oxymes (diacetyl monoxime), in strong acids in the presence of TSC. The protocol to prepare the color developed reagent (COLDER) has been described elsewhere [47] and applied to detect the enzymatic activity of PADI4 [30,48]. We also used to monitor the citrullination the modification of the COLDER reaction in the presence of antipyrine [49], which yields a yellow compound instead of a red-pink one.

All absorption spectra were recorded between 400 and 600 nm on an UV-Visible spectrophotometer Shimadzu UV-1603 by Shimadzu (Kyoto, Japan) at room temperature. Water was used as a reference for the blank subtraction.

We used the same procedure and protocols described elsewhere [30]. All the controls and the reactions were made in duplicate for each of the reagents (COLDER alone, and COLDER modified with antipyrine). The control experiments were repeated twice. The “reaction buffer” contained 100 mM Tris (pH 7.6), 50 mM NaCl, 2 mM DTT and 10 mM $CaCl_2$ up to a final volume of 500 μL. To the tubes containing the “reaction buffer”, except the one containing water, we added PADI4 from a stock solution, to yield a final concentration of 0.75 μM (in protomer units). No PADI4 was added to the blank solution containing only water. Next, to the test tubes containing PADI4, we added a volume from a stock solution of SAA to yield a final concentration of 100 μM. The resulting solutions were incubated for 25 min at 37 ºC in an Innova 4000 new Brunswick scientific incubator (Thermofisher, Madrid, Spain) with a 190 rpm shaking. After such period, we added BAEE from a stock solution to yield a final concentration of 100 μM. The control tube containing only L-citrulline had a final concentration of 100 μM. Control experiments in the presence of 100 μM of GSK484 with PADI4 (0.75 μM in protomer units) and BAEE (100 μM) were also carried out.

Next, samples were incubated at 37 ºC for 25 min in the same shaker with agitation. Reactions were quenched by flash freezing in liquid nitrogen. For color development, 2 mL of freshly prepared COLDER solution were added to the quenched reaction, vortexed to ensure complete mixing, and incubated for 15 min at 95 ºC; the same amount of reagent containing antipyrine was added to the other tubes in parallel. After cooling at room temperature, the samples were transferred into 1 mL-quartz cuvettes to be measured in the UV-spectrophotometer.

2.8. Molecular modelling experiments

Molecular docking experiments were performed with the software YASARA [50,51] applying the incorporated AutoDock Vina algorithm [52]. For SAA, only the R enantiomer was considered, corresponding to the natural form isolated from *Salvia miltiorrhiza*, whose biological activity has been extensively described [9]. The 3D conformer structure file (SDF format) was downloaded from Pubchem (https://pubchem.ncbi.nlm.nih.gov/compound/5281793) and directly used for docking studies. The dimeric structure of PADI4 was retrieved from the Protein Data Bank (PDB number 3APN) [53]. The selected protein structure underwent a standard cleaning and optimization procedure to ensure optimal conditions for molecular docking experiments, adding all existent hydrogen atoms and adjusting the charge. A physiological pH value of 7.4 was used in the simulation, at which most amino acids have neutral side-chains, except arginine and lysine (both positively charged), aspartate and glutamate (both negatively charged) and histidine, which may occur in either a neutral or a positively charged state depending on its local environment. The N- and C-terminal residues were assigned with positive and negative charges, respectively.

A global docking was performed with 999 runs, the maximum permitted by YASARA. The docking grid-box was defined to include half of each monomer of the head-to-tail antiparallel PADI4 homodimer. In this way, the full dimer is represented by symmetry without overlapping redundant regions to optimize the calculations. This configuration ensures coverage of all relevant binding regions while avoiding redundant sampling of symmetrical areas. The protein was kept rigid, whereas the ligand was flexible during docking to optimize its conformation in the binding pose. After the docking calculations, the results were treated by using YASARA, which enabled the evaluation of the binding scores and the clustering of poses. Poses with a root-mean-square deviation (RMSD) lower than 5 Å were grouped into the same cluster, and a representative pose was generated for each cluster and exported into PDB format.

To analyze the relative position of the clusters, pairwise RMSD analysis between clusters was performed and represented in form of heatmaps. RMSD calculations between representative poses, and interaction profiling was carried out by using in-house Python scripts based on the MDAnalysis and ProLIF libraries, which were used solely for structural analysis and not for a molecular dynamics trajectory processing. Differences in RMSD were further analyzed by hierarchical clustering dendrograms. Residue interactions with the ligand observed in at least four representative structures occupying the potential binding region were identified, including different kinds, such as hydrogen bonds, hydrophobic, π–π stacking, cation–π, anion–π, π–cation / π–anion, salt bridges, metal coordination, halogen bonds and water bridges. Additionally, the ligand radius of gyration (R_g) and its solvent-

accessible surface area (SASA) were calculated for each representative docking pose to evaluate the stilbenoid compactness and its degree of burial within the dimerization interface. The R_g values were computed from the ligand heavy atoms. These analyses were performed by using in-house scripts implemented in Python [54,55], including libraries such as MDAnalysis (v2.4.0) [56,57] and ProLIF (v.1.0.0) [58] and implementing different algorithms, specifically Kernel Density Estimation [55]. The SASA values were obtained by using the available online server dr_sasa (http://schuellerlab.org/dr_sasa/) [59].

Molecular dynamics simulations were carried out to monitor the temporal evolution of the best protein–ligand system obtained from the docking predictions. The system was simulated for 100 nanoseconds (ns) using YASARA [50,51]. The simulation cell included a 5 Å buffer in all directions, and calculations were performed with the AMBER14 force field in TIP3P water containing 0.9 % NaCl. System neutrality was achieved by adding the required counterions, and the temperature was kept constant at 25 °C through the simulation. The number of atoms used in each chemical moiety employed during the simulation are shown in Table 1.

Trajectory analysis was performed by using YASARA functionalities. These analyses provided key descriptors related to complex stability and interaction patterns over time, such as the percentage of secondary structure. Moreover, the RMSD during the simulation was computed to assess the structural stability of the protein–ligand complex relative to its initial reference conformation. Root Mean Squared Fluctuation (RMSF) was also obtained to quantify the movement of protein side-chains. In addition, interactions were computed along the trajectory at 0.1-ns intervals to monitor the temporal evolution of protein–ligand contacts. This analysis enabled the study of the persistence and frequency of interactions established with individual residues of each monomer, providing a detailed description of the dynamic binding pattern through the whole simulation.

2.9. Cell lines

The primary human GBM cell line HGUE-GB-39 (hereafter referred to as GB-39) was isolated from surgical washes as reported previously [60]. Colorectal cancer (SW-480) cell line was donated by Instituto Municipal de Investigaciones Médicas (IMIM, Barcelona, Spain) [61]. The SW-480 cell line was cultured in Dulbecco's Modified Eagle's Medium-High Glucose (DMEM-HG) (Biowest, MO, USA). GBM cells were cultured in Dulbecco's Modified Eagle's Medium-Nutrient Mixture F-12 (DMEM F-12) (Biowest, MO, USA). Both media were supplemented with 10 % (v/v) heat-inactivated fetal bovine serum (FBS) (Capricorn Scientific, Ebsdorfergrund, Germany) and 1 % (v/v) penicillin/streptomycin mixture (Biowest, MO, USA). The cells were then incubated at 37 °C in a humidified atmosphere containing 5 % CO_2.

2.10. Proliferation assay

The cell lines described above were seeded in 96-well standard plates (Sarstedt, Nümbrecht, Germany) with a density of 4.000 cells/well and incubated at 37 °C in the presence of 5 % CO_2 for 24 h. Subsequently, cells were treated with increasing concentrations of SAA (in the range 2–100 μM) for 72 h under the same conditions. Then, in any of the experiments, 0.25 mg/mL of MTT were added and the samples were incubated for 3 h; afterwards, the medium was removed and 100 μL of DMSO were added. The plate was shaken at room temperature for 20 min to dissolve the formed formazan crystals. Finally, the absorbance was measured on an Eon™ Microplate Spectrophotometer (BioTeK®, Winooski, VT, USA) at 570 nm.

Table 1
Number of atoms used in the simulation.

Chemical moeity	Number of atoms
Protein	17,669
Ligand	56
Element Na	233
Element Cl	230
Water	248,019
Total	266,207

2.11. Proximity ligation assay (PLA)

An amount of 35.000 cells of the GB-39 cell line were seeded in 24-well plates on coverslips. After 24 h, cells were washed in phosphate buffered saline (PBS) (1 ×), fixed with PFA 4 %, washed again, permeabilized in PBS (1 ×) with 0.2 % Triton X-100, and blocked with blocking solution for 1 h at 37 °C before immune-staining with Duo-link by using PLA Technology (Merck, Madrid, Spain), following the manufacturer's protocol. Anti-PADI4 (1:200 mouse, Abcam) and anti-RING1B (1:100, rabbit, Abcam) primary antibodies were used. Then, slides were processed for *in situ* PLA by using sequentially the Duolink In Situ PLA Probe Anti-Mouse MINUS, Duolink In Situ PLA Probe Anti-Rabbit PLUS, and Duolink In Situ Detection Reagents Red (Merck, Madrid, Spain). In these experiments, red fluorescence spots correspond to the PLA-positive signal, and they indicate that the two proteins are bound, forming a protein complex, whereas the blue fluorescence signals correspond to nuclei (DAPI staining). Both negative and positive control experiments were performed, the former by omitting one of the primary antibodies. Image acquisition was carried out by using a confocal microscope LSM900 with Airyscan 2 (Carl Zeiss, Oberkochen, Germany) at 63 × magnification.

2.12. Statistical analyses

To evaluate the normal distribution of the data, either in PLA or in the proliferation assays, the Shapiro–Wilk statistical test was used. The two-way ANOVA followed by Tukey's *post hoc* test was used to analyze the association between variables. Differences were statistically significant with a p-value < 0.05, and significant changes were indicated as follows: the "*" is used for p-value < 0.05; the "**" for p-value < 0.01; the "***" for p-value < 0.001; and the "****" for p-value < 0.0001. Statistical analysis was performed with GraphPad Prism v7.0a software (GraphPad Software Inc., San Diego CA, USA).

3. Results

3.1. SAA bound to PADI4 in vitro

To test whether PADI4 interacted with SAA *in vitro*, we followed a two-part experimental approach. To observe a possible binding, and concomitant conformational changes in PADI4 upon binding, we used the spectroscopic techniques steady-state fluorescence, far-UV CD and NMR. Once binding was ascertained, we used ITC and fluorescence to quantitatively measure the thermodynamic parameters of such binding.

We used fluorescence to determine whether there was a change in: (i) the position of the maximum wavelength; (ii) the intensity at such wavelength; or (iii) both, when the spectrum of the complex was compared to that obtained from the addition of the separated spectra of the two isolated molecules. SAA did not show a fluorescence spectrum after excitation at 280 nm, but rather when it was excited at 370 nm (data not shown). On the other hand, a variation in fluorescence intensity after excitation at 280 nm was observed when the complex of PADI4 with SAA in excess was formed, but there were no changes in the maximum wavelength of the spectrum (Fig. 1 A).

We also carried out fluorescence thermal denaturations of: (i) the complex formed between PADI4 and SAA; and (ii) PADI4 in isolation. In both cases, the denaturations were irreversible, but the thermal denaturation midpoint for isolated PADI4 was 325 (52 ° C) ± 1 K, and that for the complex with SAA was 331 (58 ° C) ± 4 K (Fig. 1 B). Then, both

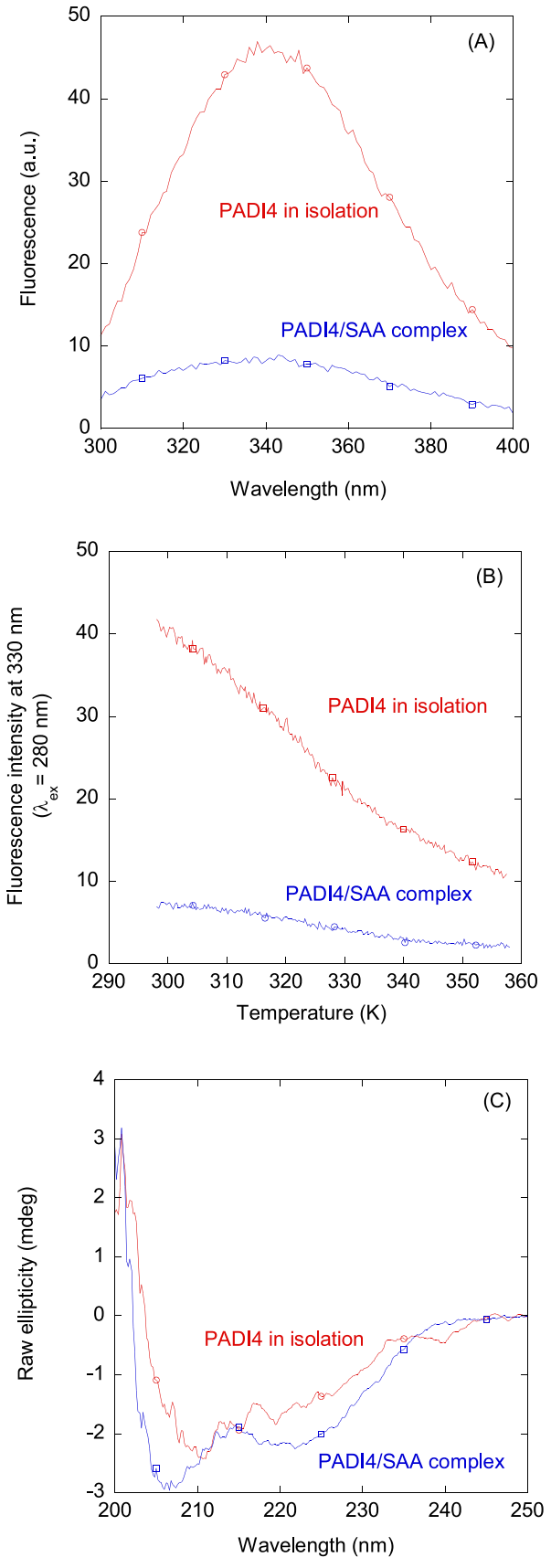

(caption on next column)

Fig. 1. Binding of SAA to PADI4 monitored by different biophysical probes. (A) Fluorescence spectrum obtained by excitation at 280 nm of the PADI4/SAA complex, and addition spectrum obtained by the sum of the spectra of the two isolated molecules (SAA in isolation did not show an emission fluorescence spectrum). (B) Thermal denaturation of isolated PADI4 and the PADI4/SAA complex followed by fluorescence after excitation at 280 nm. (C) Far-UV CD spectrum of the PADI4/SAA complex, and addition spectrum obtained by the sum of the spectra of the two isolated macromolecules (SAA in isolation did not show a far-UV CD spectrum). All experiments were performed at 25 ºC.

fluorescence steady-state experiments and thermal denaturations indicated that there was binding between SAA and PADI4.

Next, we carried out far-UV CD measurements, with the aim of further supporting the results obtained by fluorescence. The far-UV addition spectrum (obtained by the sum of the spectra of PADI4 and SAA) was different to that of the complex (Fig. 1 C). The differences could be either attributed to a relatively large number of aromatic residues of PADI4 involved in the binding (even those aromatic rings present in the structure of SAA, Fig. 1), or alternatively to conformational changes of PADI4 when bound to SAA. In any possible scenario, the far-UV CD spectra indicated binding between both molecules.

Since we have showed, by using fluorescence and far-UV CD, that there was binding between SAA and PADI4, we carried out fluorescence titrations to quantitatively measure the binding affinity of the reaction. The results indicate that the dissociation constant was 7 ± 3 μM (Fig. 2 A). We also used ITC to determine the thermodynamic binding parameters, *i.e.*, the enthalpy and the entropy of the binding reaction between SAA and PADI4 (Fig. 2 B). According to the calorimetric experiments, the dissociation constant, K_d, for the interaction of PADI4 with SAA was 620 ± 40 nM, accompanied by an enthalpic contribution of −8.3 ± 0.3 kcal mol^{-1}, indicating that there was a net entropic contribution of 0.59 cal mol^{-1} deg^{-1}. The stoichiometry of the complex as determined by ITC was close to 1.6:1 (in protomer units of PADI4).

Finally, we confirmed the binding by using WaterLOGSY NMR experiments. In the presence of PADI4, the signals of SAA appeared inverted, when compared to the same signals in the control experiment (Fig. S1) or the signals of DTT, glycerol and EDTA (all of which appeared as positive). This inversion was observed especially on the aromatic part of the molecule, namely the signals between 6 and 8 ppm. Aliphatic signals of the -CH_2- group located at the center of the SAA molecule (Fig. 1) seemed to be less affected (Fig. S1).

Taken together, all the biophysical probes indicate that SAA was bound to PADI4 with a medium to nanomolar affinity.

3.2. SAA was bound to PADI4, but it did not do so at the active site of PADI4

We have shown that there was binding between PADI4 and SAA, but we were interested also in elucidating whether binding occurred at the active site or at another different position of the enzyme. In this case, we used a two-part approach.

First, we determined whether SAA was competing by the active site with a natural substrate of the protein: the C-terminal region of RING1B (C-RING1B), comprising residues 228–336 [33]. It is important to indicate that we are using the C-RING1B, the C-terminal region of RING1B (residues 228–336 of the intact RING1B protein), as a reporter protein. We have previously shown that C-RING1B binds to the PADI4, through its active site and it is a substrate [33]. The C-RING1B is a well-folded protein, with a well-dispersed 2D ^{1}H-^{15}N HSQC spectrum. Previous works show that some of the cross-peaks in the spectrum of C-RING1B are changed in the presence of an excess of PADI4, but these changes can be reverted to the original chemical shifts observed in isolated C-RING1B, in the presence of GSK484, an inhibitor of the enzyme [33]. Therefore, we wondered, whether cross-peaks in the spectrum of C-RING1B would move towards the chemical shifts observed in the free, isolated domain upon addition of equimolar

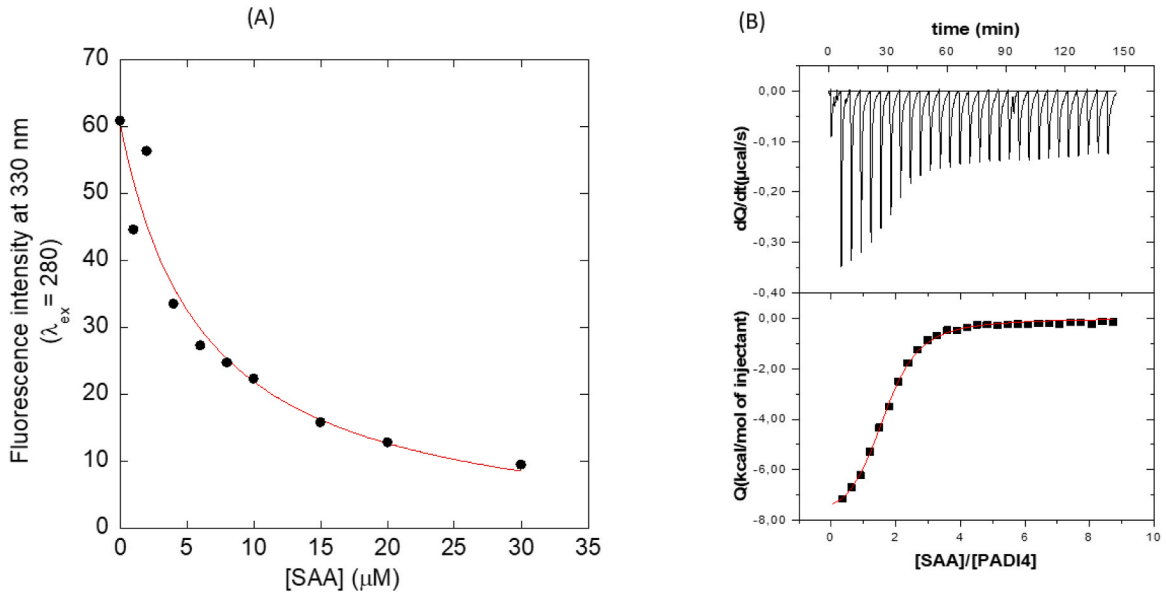

Fig. 2. Quantitative determination of the binding of SAA to PADI4 monitored by different biophysical probes. (A) Titration curve monitoring the changes in the fluorescence at 330 nm when SAA was added to PADI4 at 25 ºC. The fluorescence intensity on the y-axis is the relative signal after removal of the corresponding blank. The line through the data is the fitting to Eq. (1). (B) Calorimetric titrations of SAA with PADI4 at 25 °C in buffer Tris 20 mM (pH 7.6), glycerol 10 % (vol/vol), 1 mM EDTA, TCEP 0.5 mM and 150 mM NaCl. The lower graphic shows the heat integrated in each injection. The upper panel shows the thermograms (thermal power as a function of time), and lower panels show the binding isotherms (ligand-normalized heat effects per injection as a function of the molar ratio in the calorimetric cell). Continuous line corresponds to the fitting curve according to a single ligand binding site interaction model.

amounts of PADI4 and SAA. In our experiments, we observed that the presence of PADI4 caused changes in the chemical shifts of many cross-peaks of the spectrum of C-RING1B (red spectrum), thus confirming previous results [33]. These changes were of two types: (i) some of the cross-peaks of the spectrum of C-RING1B disappeared, due to the larger molecular weight of the complex formed (Figs. 3 and S2); and, (ii) other peaks showed a decrease in the signal intensity, together with changes in chemical shifts (Figs. 3 and S1). This different behavior among the cross-peaks indicated that the binding between the two proteins was specific, and occurred at polypeptide patches of both proteins, namely at the active site of PADI4 (Cys645) and around Arg231 of C-RING1B [33]. On the other hand, upon addition of an equimolar amount of SAA to the solution containing C-RING1B and PADI4, we observed that there were changes in the chemical shifts and in the broadening of some cross-peaks of the 2D ^{1}H-^{15}N HSQC spectrum of C-RING1B, when compared to that of the PADI4/C-RING1B complex

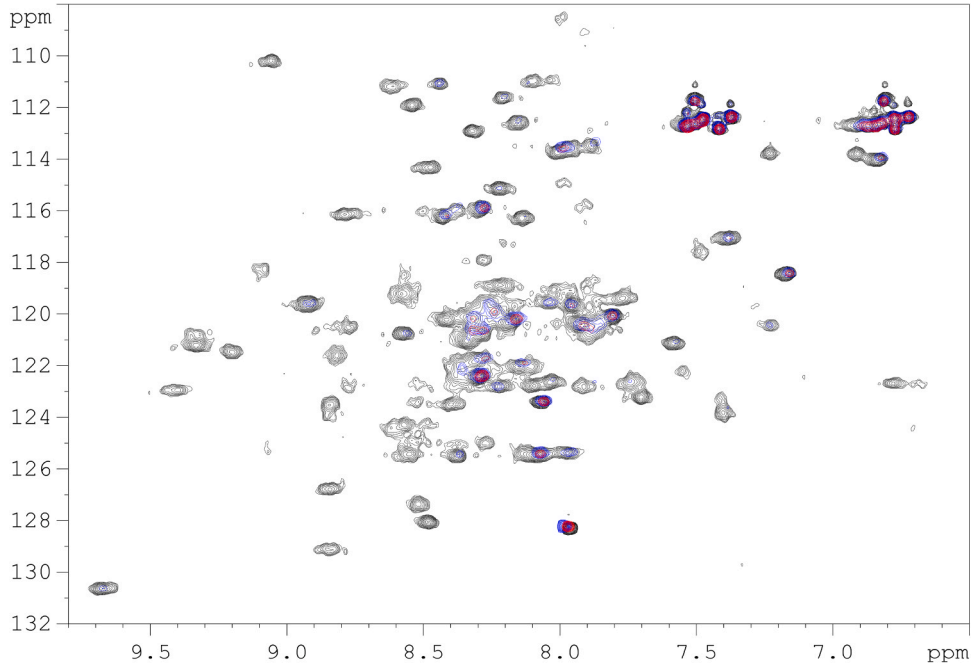

Fig. 3. 2D ^{1}H-^{15}N HSQC NMR spectra to monitor the association of PADI4 and SAA, in the presence of C-RING1B. 2D 1H-15N HSQC NMR spectra of C-RING1B in the absence (black lines), in the presence of PADI4 (red lines), and when PADI4 was present together with the SAA at equimolar amounts (blue lines). The same lower contour level was used for all the spectra. All experiments were carried out at 25 C.

(Figs. 3 and S1). However, the changes were not as important as those occurring in the presence of GSK484 [33]; furthermore, those changes did not revert to the original chemical shifts and broadening of the cross-peaks of the spectrum of isolated C-RING1B. These findings suggested that C-RING1B and SAA were not competing for the same site of PADI4, and since C-RING1B is a substrate of the PADI4, binding of SAA should occur at a place different of the active site of PADI4. However, it is important to indicate that the conclusion on the findings of these experiments could be skewed if SAA was capable of binding to C-RING1B. To that end, we carried out fluorescence control titration experiments of isolated C-RING1B with SAA, and we obtained an estimated K_d of ~ 20 μM (data not shown); therefore, binding of SAA to the C-RING1B occurred as well. Thus, although the affinity of SAA for C-RING1B was smaller than for PADI4 (Fig. 1), we cannot rule out that the effects observed in the above NMR spectra could be also due to binding of SAA to C-RING1B.

And as a second approach, we hypothesized that if SAA was aiming to the active site of PADI4 — conversely to what seems to be inferred from the NMR experiments —, the citrullination of BAEE by the enzyme would be hampered, as it happens when using GSK484; thus, if SAA was aiming to the active site of PADI4, we should not observe a citrullination of BAEE, and then, lack of color development. SAA did not hamper the citrullination of BAEE (as GKS484 does), resulting in UV spectra with lower absorbance intensity (and less amount of formed citrulline). Rather, the UV spectra of BAEE in the presence of PADI4 and SAA had a higher intensity, as shown by either the COLDER agent or in the presence of antipyrine, than when PADI4 and BAEE were present in the solution. Then, we can conclude that SAA was an activator of citrullination (Fig. 4).

To sum up, SAA was bound to PADI4, but such interaction did not seem to involve the active site of the enzyme, but rather another allosteric site related to an activation of citrullination.

3.3. SAA bound to PADI4 in silico at the dimeric interface

To obtain more information about the PADI4 binding site of SAA, and due to the large size of the formed complex, we carried out molecular docking studies *in silico* on the PADI4 dimer and a molecular dynamics (MD) simulation. Docking of the ligand against the enzyme using YASARA produced 999 poses with binding scores ranging from approximately + 10.0 to + 10.7 kcal mol^{-1}, where higher values indicate tighter affinity. A Gaussian-kernel density estimate (Fig. 5 A) identifies two primary peaks at approximately + 10.3 and + 10.5 kcal mol^{-1}. Clustering of all poses based on RMSD — with those exhibiting an RMSD below 5 Å to one another being grouped into the same cluster as detailed in the Materials and Methods section — resulted in nine clusters (1–9) with similar mean scores (Fig. 5 B). Each cluster presented a representative compound pose (RC1–RC9). Pairwise RMSD analysis of the representative poses (Fig. 5 C) revealed a clear separation of cluster RC3 from the rest of the ensemble. Specifically, RC3 displayed RMSD values exceeding 25 Å when compared to all other cluster representatives, indicating a markedly distinct binding orientation. In contrast, the remaining eight clusters (RC1, RC2, RC4–RC9) exhibited a high degree of structural similarity, with mutual RMSD values consistently below 10 Å. This finding suggested a dominant and conserved binding mode among most of the clusters, while RC3 likely represented an outlier pose with limited relevance to the predominant binding behavior. Average-linkage clustering of the RMSD matrix (Fig. 5 D) further assembled the eight high-scoring centroids into two tightly related subfamilies, with RC3 consistently isolated on the most distal branch. Structural representation onto the receptor backbone (Fig. 5 E) visually confirmed that eight conformers converged on the same inter-monomer cleft whereas RC3 extended into an adjacent groove. Thus, these data confirm a single, potential binding mode and identify RC3 as an outlier likely originating from the sampling process, or alternatively, scoring limitations rather than a novel binding site.

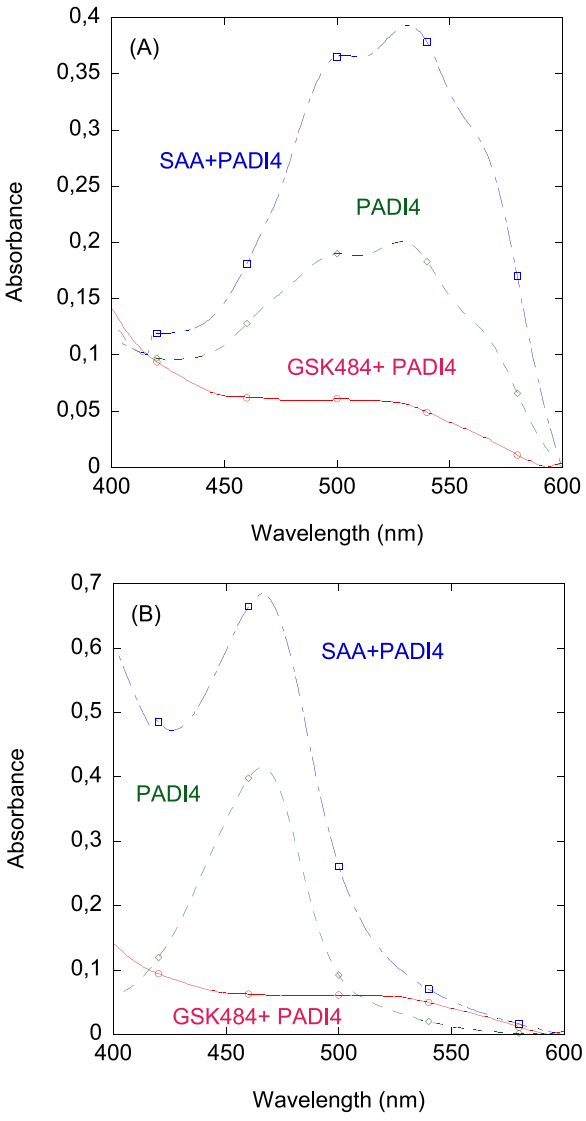

Fig. 4. Colorimetric citrullination assays of BAEE in the presence of PADI4 and SAA, in (A) Colorimetric (COLDER) assays of BAEE for samples containing GSK484 (a well-known inhibitor of PADI4) and PADI4 (red); only PADI4 (green); and PADI4 with SAA (blue). (B) Colorimetric assays of BAEE in the presence of antipyrine for samples containing GSK484 (a well-known inhibitor of PADI4) and PADI4 (red); only PADI4 (green); and PADI4 with SAA (blue) All experiments were carried out at 25 C.

To further characterize the structural features of each representative pose, we analyzed the ligand R_g and its SASA, as reported in Supplementary Table 1 (Table S1). RC1 exhibited the lowest solvent-exposed surface (53.5 $Å^2$) and a compact conformation (R_g = 5.93 Å), indicating that this pose is the most deeply buried within the dimerization interface. Such a high degree of burial indicates that the ligand was deeply accommodated within the dimerization interface, suggesting that its binding might stabilize the interaction between both monomers, and thereby favoring dimer formation. Most configurations displayed intermediate burial (70–110 $Å^2$) and comparable R_g values, reflecting similar orientations within the same inter-monomer cleft. In contrast, RC3 showed the highest SASA (148.5 $Å^2$) and a lower R_g (4.75 Å), corresponding to a more exposed and spatially confined binding mode likely associated as a potential outlier conformation.

A detailed interaction analysis was carried out for the representative structures of clusters RC1 to RC9, except RC3, which was excluded due to its classification as an outlier (see above) (Table S1). The most

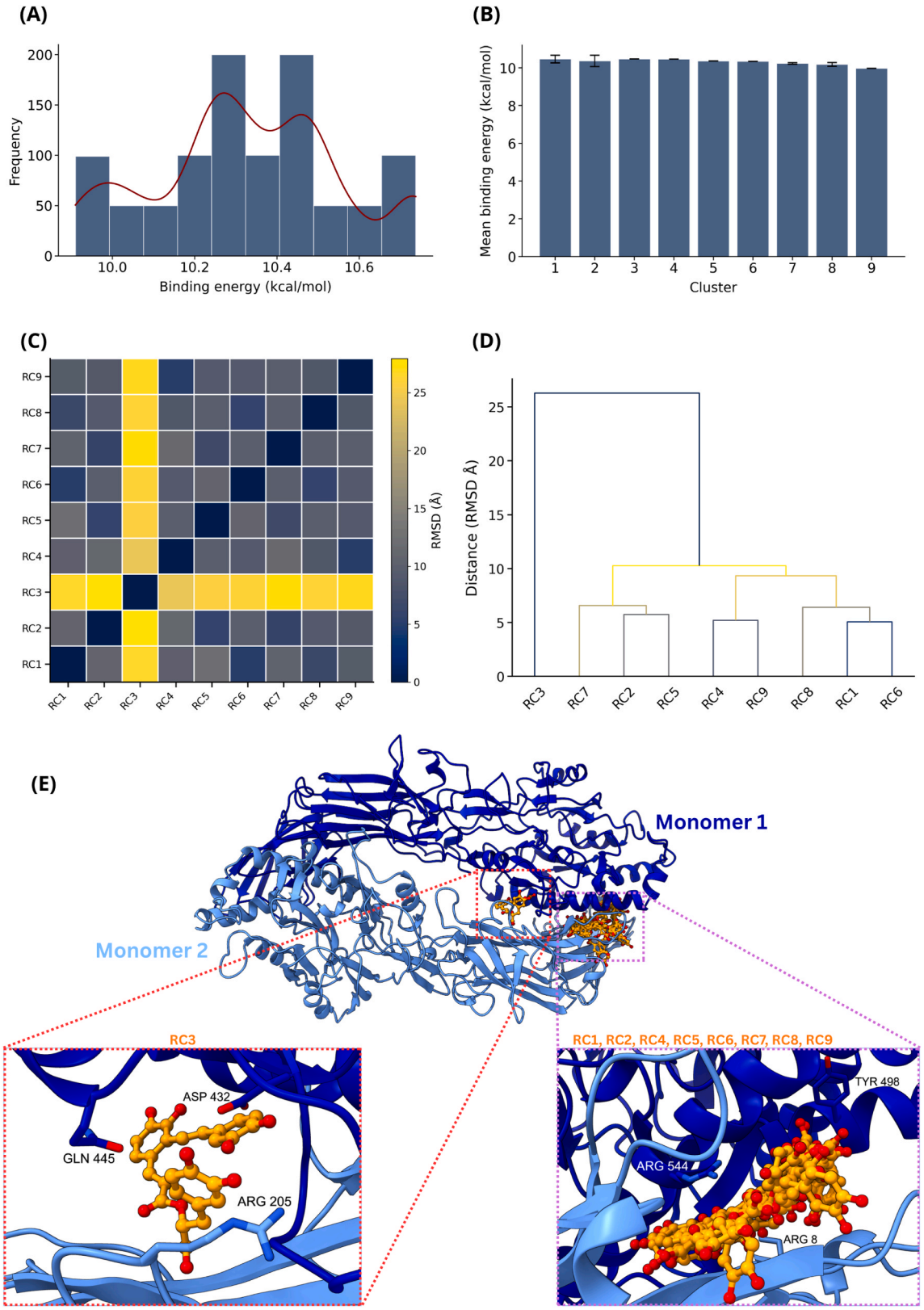

Fig. 5. Conformational diversity and clustering of ligand-dimer binding poses in docking studies between PADI4 and SAA. (A) Histogram of binding energies for all 999 docking poses overlaid with a Gaussian kernel density estimate. (B) Mean binding energy for each of the nine clusters (1–9) ± standard deviation (bind-energy spread). (C) Pairwise RMSD heatmap (Å) between cluster representative structures (RC1-RC9), colored on a "cividis" scale from 0 Å (dark blue) to highest observed RMSD (yellow). (D) Hierarchical clustering dendrogram of the nine cluster representatives based on their RMSD distances, with branches colored by RMSD linkage by using the same "cividis" palette; vertical axis denotes RMSD in Å. (E) Representative overlay of all nine cluster centroids (RC1-RC9) onto the dimer receptor (light blue and dark blue cartoon), with ligand heavy-atom traces shown as orange ball and sticks, illustrating the spatial distribution of binding modes across the dimer interface. Zoom squares provide detailed representation of the two different binding regions, indicating protein residues, and which RCs belong to each region.

recurrent interactions, that is, those observed in at least four of the representative cluster structures, are summarized in Fig. 6 A and 6 B. The interaction profile shown in Fig. 6 A highlights a consistent network of van der Waals and hydrophobic contacts, suggesting a degree of conservation in the binding mode across multiple poses. This is not unexpected, as SAA has a large, non-polar surface. Notably, van der Waals contacts involved residues such as Gln13, Thr10, and Tyr498, whereas hydrophobic interactions were associated with non-polar side chains, such as Leu6 and Ala17, contributing to the stabilization of the ligand within the pocket. Interactions took place simultaneously with amino acids from both monomeric chains of the dimer (indicated by indexes 1 and 2 in Fig. 6 A), placing the ligand on the dimer interphase.

Fig. 6 B provides a two-dimensional map of the molecular interactions within the top one representative SAA binding conformation. This diagram further emphasizes the structural coherence of the binding site, particularly around two aromatic moieties of the ligand, which form key interactions with surrounding residues. This result agrees with the WaterLOGSY results (Fig. S1), where the effect was mainly observed on the aromatic region of the molecule (Section 3.1).

Fig. 6 C provides a tridimensional image of the binding pocket of the energetically most favorable pose that belongs to the cluster RC1. Interactions with Arg544 and Arg8, as well as Asp273 and Asp547 are labelled. These residues have been previously identified as being essential for the interaction of both PADI4 monomers to form the dimer [62], while none of them belongs, or is close to, the active center of the protein [63]. These findings suggest that ligand binding in this region might influence protein–protein interactions rather than directly affecting enzymatic activity: dimerization has been shown to be a key factor in PADI4 activity, as it is required for cooperative calcium binding [62].

To assess the stability and dynamic relevance of the predominant binding mode identified through docking, we performed a 100-ns all-atom MD simulation of the PADI4 dimer in complex with SAA by using the representative pose RC1. This simulation allowed us to evaluate the temporal persistence of key contacts within the complex and the structural response of the binding interface under explicit-solvent conditions.

The Fig. 7 A shows that the backbone RMSD of PADI4 rapidly stabilized within the first few nanoseconds of the trajectory and remained between approximately 2.5 and 3.5 Å of the initial conformation for the rest of the simulation. This behavior indicates that the head-to-tail dimer maintained a stable global conformation throughout the 100-ns timescale, with no evidence of unfolding or, alternatively, large-scale rearrangements.

Local flexibility patterns were examined through *per*-residue RMSF analysis (Fig. 7 B). Most of the residues displayed fluctuations below 2 Å, consistent with a structurally stable enzyme. Higher mobility was observed in loop regions and terminal segments, which is typical for large dimeric enzymes, but such mobility did not compromise the integrity of the binding interface. Importantly, residues forming the inter-monomer cleft remained relatively rigid, supporting the idea that this region could accommodate ligand binding without undergoing serious structural disruption.

The secondary structure profile remained remarkably constant over the trajectory (Fig. 7 C). The relative proportions of α-helix, β-sheet, turn, and random-coil elements showed minimal variation, demonstrating that the overall fold of each monomer was preserved and further confirming the structural robustness of the dimer.

A detailed analysis of protein-ligand interactions is presented in Supplementary Figure 3. In monomer A (Fig. S3 A), the ligand established persistent hydrophobic and hydrogen-bond contacts with residues located at the dimerization interface, remaining engaged with this surface throughout the whole simulation. In contrast, contacts with monomer B (Fig. S3 B) were more transient and less frequent. This interaction profile indicated that the ligand preferentially associated with one side of the inter-monomeric cleft, whereas maintaining intermittent contacts with the facing monomer.

Overall, these MD results confirmed that SAA remained stably bound at the dimerization interface of PADI4, dynamically exploring the inter-monomeric cleft without detaching, in agreement with the binding mode suggested by the docking.Finally, our results *in silico* indicated that the effect of SAA on PADI4 activity, as detected by the colorimetric (COLDER) reaction, must be related to dimer stabilization.

3.4. SAA effect on viability varied among different cancer cells

It has been previously described that SAA exhibits antitumor properties in U87 glioma cells after 24 and 48 h of treatment [64]. Therefore, we tested the effect of increasing the concentration of SAA (in the range 2–10 μM) on the patient-derived GBM cell line GB-39 (Fig. S4). As there was no significant reduction in cell viability upon treatment, we increased the SAA concentration to 100 μM. Although a significant decrease in cell viability was observed at the highest SAA concentration, this was insufficient to reach the IC_{50} (Fig. 8 A).

SAA also impacts the occurrence and development of tumors such as melanoma or breast cancer by influencing cell migration, invasion, apoptosis and proliferation [11,65,66]. Hence, we studied the possible role of SAA in other types of cancer, such as COAD, by using the SW-480 cell line. Like in GBM, we observed a statistically significant decrease in SW-480 cell viability at SAA low concentrations, in accordance with previous reports in other COAD cell lines (Fig. 8 B) [67].

Interestingly, previous reports indicated that, although SAA affected COAD cell viability less than other natural compounds, such as platycodin D or diosmin, treatment with 30 μM SAA inhibited the glucose regulated protein 78 (GRP78) secretion more than the treatment with the other compounds, yielding to angiogenesis inhibition [67]. These results suggest that SAA may exert anticancer effects by influencing other critical processes in cancer. For instance, it has been proposed that SAA interacts with GRP78 in the cytosol, directing the protein to enter the lysosomal degradation pathway [67].

Therefore, we speculate that similarly to the ability of SAA to inhibit GRP78 secretion and then, altering the tumor microenvironment suppressing angiogenesis in COAD, other key processes might also be affected in GBM cell lines upon SAA addition.

3.5. SAA blocked the binding of PADI4 to RING1B in cellular assays

To corroborate the SAA binding to PADI4 *in vitro*, we used the Duolink In situ assay. This technique, known as proximity ligation assay (PLA), detects protein binding at distances shorter than 16 Å, and visualizes the interaction within cell compartments as red fluorescent spots.

Based on the SAA/PADI4 affinity constant calculated by ITC (600 nM) (Fig. 9), we selected an intermediate SAA concentration of 2 μM to treat the GBM cells. As the interaction in the untreated cells was mostly observed in the cytoplasm, it is worth noting the shift in location to more nuclear positions after 6 h of SAA treatment, even though the total number remained unchanged. After 24 h in the presence of SAA, PADI4/RING1B interactions in GB-39 cells were almost completely abolished, with only a residual signal remaining in the nucleus (Fig. 9).

It has been reported that PADI4 and RING1B were interacting through the active site of the enzyme [33]. According to our results *in vitro* (Fig. 4) and *in silico* (Figs. 5, 6 and 7), the binding of SAA did not seem to occur at the PADI4 active site. Therefore, we speculate that the hampering of the PADI4/RING1B interaction observed in our results in the experiments using GBM cells must occur through an allosteric mechanism.

4. Discussion

In the search for new lead compounds targeting diseases, natural products have unique advantages in terms of availability and scaffold

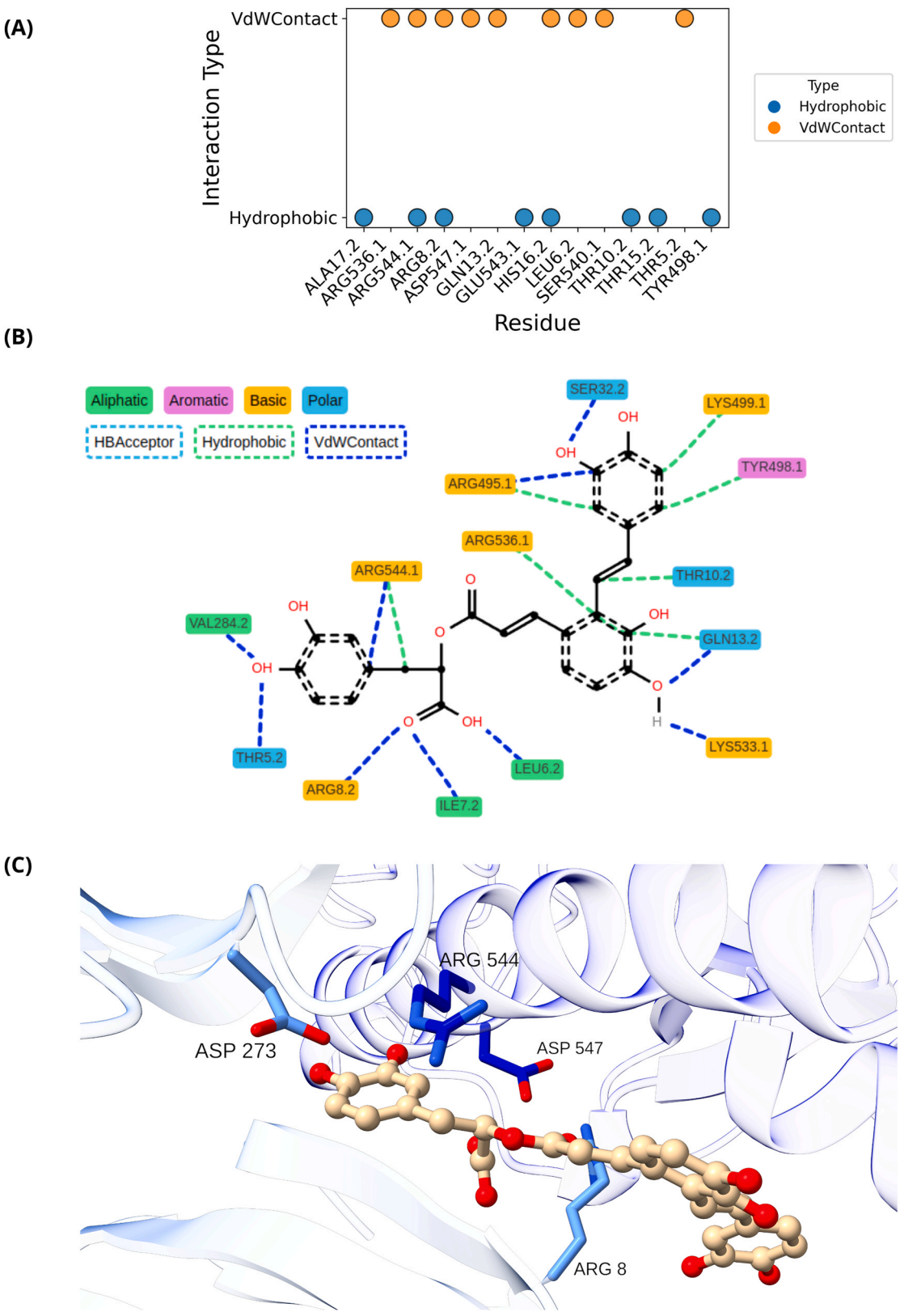

Fig. 6. Interaction profile and structural view of the top-scoring ligand pose in PADI4/SAA complex. (A) Residue interactions observed in at least four out of eight high-affinity representative structures that occupy the potential binding region. Hydrophobic contacts (blue circles) and van der Waals contacts (orange circles) are plotted against residue identity, highlighting a conserved interaction network. Indexes 1 and 2 indicate monomer chains 1 and 2, respectively. (B) Two-dimensional interaction diagram for the single best-scoring pose, showing hydrogen bonds (green dashed lines), hydrophobic and van der Waals contacts color-coded by residue class (aliphatic, aromatic, basic, polar). Residue labels correspond to residue number. Indexes 1 and 2 indicate monomer chains 1 and 2, respectively. (C) Three-dimensional representation of the highest-scoring binding representative structure. Ribbon representation of the PADI4 dimer (dark and light blue), with SAA shown in sticks.

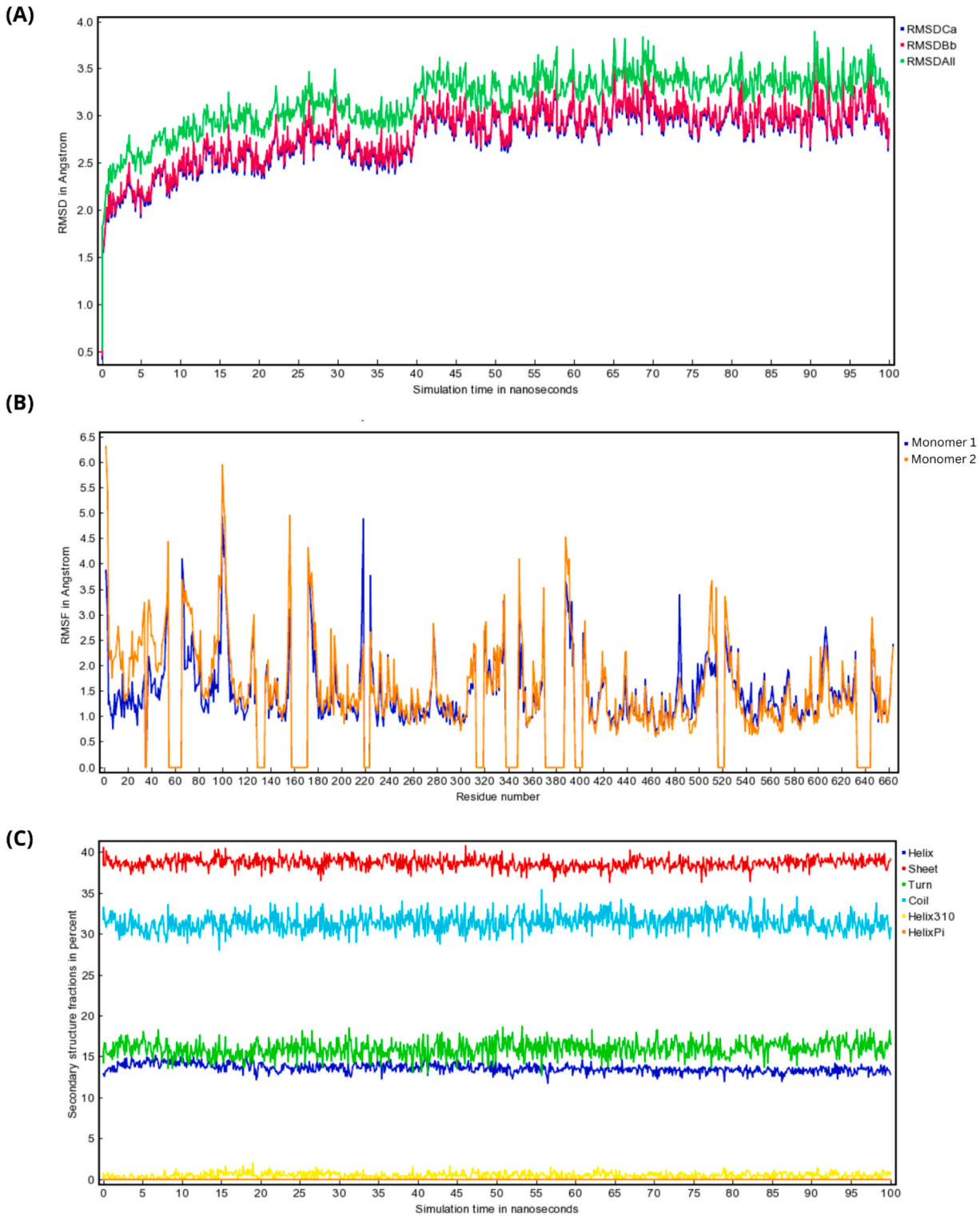

Fig. 7. Structural stability and dynamic behavior of the PADI4/SAA complex during MD simulation. (A) RMSD of the PADI4 dimer, when forming the PADI4/SAA complex, as a function of simulation time. Three RMSD traces are shown: Cα RMSD (blue), backbone RMSD (magenta) and all-atom RMSD (green). (B) *Per*-residue RMSF profile of monomers 1 and 2 in the PADI4/SAA complex. Residue-specific fluctuations are plotted for monomer 1 (blue) and monomer 2 (orange). (C) Temporal evolution of PADI4 secondary-structure content, when forming the PADI4/SAA complex. The percentage of α-helix (red), β-sheet (cyan), turn (green), random-coil (blue), 3_{10}-helix (yellow) and π-helix (orange) is shown across the 100-ns trajectory.

diversity. *Salvia miltiorrhiza* or Danshen is one of the most important herbal medicinal drugs in TCM. It is used to treat bleeding disorders and blood stasis [68]. Salvianolic acids are, together with tanshinones (lipophilic, diterpenic quinones), the main active principles of the herbal drug. These hydrophilic derivatives are highly abundant in the roots of the plant. They have attracted interest due to their protective roles in central neuronal injuries and degeneration, probably acting on the levels of reactive oxygen species (ROS); in fact, SAA is a potent scavenger of ROS during cardiovascular injury, inhibiting the adherence of leukocytes to endothelial cells [69]. Furthermore, there is evidence of the

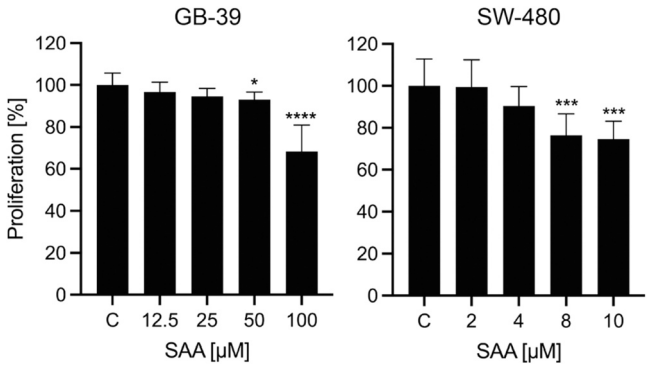

Fig. 8. Effect of SAA on cancer cell viability. Proliferation (MTT) assays with increasing concentrations of SAA in tumor lines GB-39 (left), and SW-480 (right). The results are given as mean ± standard error of the mean. Sample size n = 6. Comparison by one-way ANOVA and post hoc analysis with Dunnett's test (left) and Kruskal-Wallis test and post hoc analysis with Dunn's test (right). Statistically significant differences are indicated with asterisks (* $p < 0.05$, *** $p < 0.001$, **** $p < 0.0001$).

protective role of salvianolic acids in several cardiovascular diseases, liver fibrosis, hepatic failure and osteoporosis [68,70,71]. SAA can exert its anticancer activity through various mechanisms, such as inhibiting cell proliferation, migration, and invasion, inducing apoptosis, and modulating critical signaling pathways like PI3K/Akt, mTOR, and Wnt/β-catenin [64,66]. In agreement with previous findings that SAA could function as a multi-target agent [66], we have observed that SAA could not only bind to PADI4, but also to C-RING1B. This poses an interesting advantage as SAA could potentially circumvent the limitations of conventional monotherapies by impacting a broad range of molecular targets. Along this line, it has been described that SAA binds to the mTORC1 subunit Raptor, thereby interfering with important tumor-promoting pathways [72]. Further, SAA has been shown to inhibit some of the isoforms of human carbonic anhydrase [73], and it binds to the active site of matrix metalloproteinase-9, where it contributes to the protection of the blood-brain barrier exerting anti-inflammatory effects [74]. In some proteins, SAA favors association macromolecular process, such as in its binding to the complex transgelin/actin, triggering F-actin aggregation and improving the contractility of vascular smooth cancer cells [69]; in this macromolecular assembly, SAA binds at the interface of the transgelin/actin complex, being capable of binding to either isolated actin and transgelin. Finally, SAA can also modulate the expression and the inactivation of transgelin in several breast cancer cells by yet unknown mechanisms [65,75].

In this work, we have shown that: (i) PADI4 was capable of binding to SAA by using its dimeric interface; and (ii) the presence of the stilbenoid hampered the binding in GBM cells between RING1B and PADI4 after 24 h of compound addition.

We have shown, by using *in silico* methods, that SAA was bound in a quite stable way to the dimeric interface of PADI4, involving residues which also intervene in the dimerization of the enzyme (Table S1). This binding induced an increase in the citrullinating activity of PADI4, as judged by the findings of the colorimetric (COLDER) reactions (Fig. 4), suggesting an allosteric regulation of PADI4, by tightening the dimeric interface of the enzyme: residues involved in the scaffolding of such interface (namely, Leu6, Arg8, Asp273, Val283, Arg544 and Asp547) also showed contacts with SAA (Fig. 6, Table S1). These amino acids are not close to any of the Ca^{2+}-binding sites [76,77]. Apart from Ca^{2+}, which is an allosteric activator of PADI4 [76,78], there are not many known examples of activators of PADI4 function. Recently, peptides targeting a cleft formed by PADI4 loops Asp155-Val171 and Pro371-Pro387 have also been shown to be activators of PADI4, allowing the characterization of a new type of allosteric behavior [23], which involves specifically residues Asp165-Asp168. Therefore, we hypothesize that SAA could also act as an activator by binding to the dimeric interface of the enzyme, and then, tightening the dimerization interface. In fact, it has been shown that dimerization of PADI4 is key for full enzymatic activity and Ca^{2+} binding cooperativity [62]; moreover, it has been recently shown that different binding antibodies activate and inhibit PADI4 activity by enhancing or hampering the dimerization process [79], respectively. Enhancement of PADI2 activity has been also observed when demethoxycurcumurin, a small organic natural compound, is used, although binding does not seem to occur at the dimeric interface [80]. Moreover, the screening of compounds based in a DNA-encoded library have shown that there is a novel allosteric mechanism of inhibition in PADI2 based on binding to the dimeric interface of the enzyme [81]. Thus, it seems that the dimerization interface of PADI4 could be an allosteric region either to favor its activation or its inhibition.

In this work, we also observed that the presence of SAA hampered the binding of intact RING1B to PADI4, which is consistent with the fact that RING1B is a substrate of PADI4 [33]. However, as SAA can interact with both proteins, the presence of SAA might affect the citrullination of the RING1B by exclusively binding to PADI4, or concomitantly, to its interaction with C-RING1B at other sites of the polypeptide chain. Based on the activation of PADI4 enzymatic activity by SAA (Fig. 4), we suggest that the high promiscuity of SAA was probably behind the lack of binding between the two proteins.

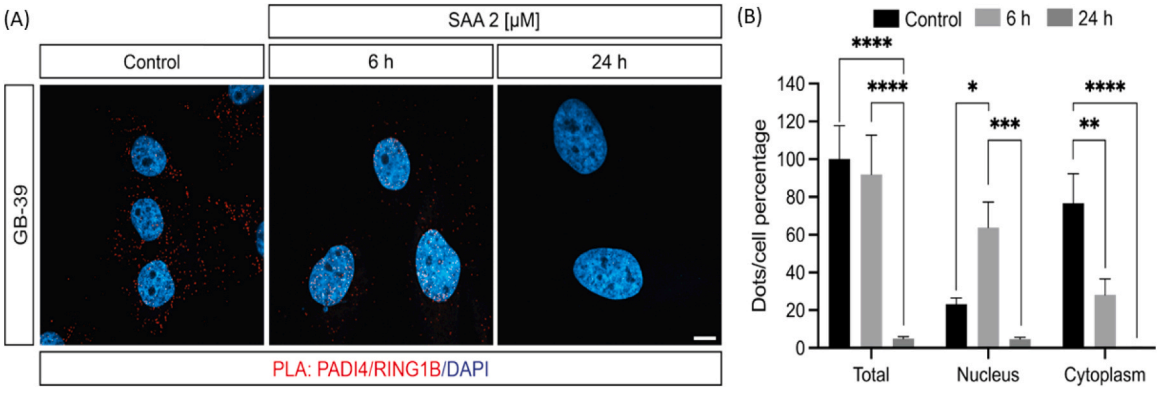

Fig. 9. Effect of SAA on the interaction of PADI4 with RING1B on the GB-39 cell line. (A) Interaction of PADI4 and RING1B upon addition of SAA at 2 μM, incubated for 6 and 24 h. Red dots indicate interactions and in blue the nuclei are observed. Sample size n = 5. (B) Quantification of the percentage of interactions per cell and subcellular compartment. Data are represented as the mean ± standard error of the mean. Comparison by two-way ANOVA and post hoc analysis with Tukey's test. Statistically significant differences are indicated with asterisks (* $p < 0.05$, ** $p < 0.01$, *** $p < 0.001$, **** $p < 0.0001$). Scale bar of 10 μM.

5. Conclusion

In this work, we have demonstrated that SAA might play a novel role in regulating the activity of PADI4 that is highly expressed in several cancers and interacts with other key oncogenic proteins such as p53, MDM2, NUPR1, and RING1B. Our findings indicate that SAA was bound with micromolar affinity to an allosteric site of PADI4, modulating its enzymatic activity and disrupting its interactions with regulatory partners such as RING1B. Interestingly, the loss of this interaction could influence key cancer process such as hypoxia, where RING1B and PADI4 have been implicated.

CRediT authorship contribution statement

Izabel Georgieva-Nikolova: Methodology, Investigation. **Felipe Hornos:** Methodology, Investigation. **Virginia Rejas:** Methodology, Investigation. **Ana Camara-Artigas:** Methodology, Investigation. **Miguel Vidal:** Resources. **José L. Neira:** Writing – review & editing, Writing – original draft, Visualization, Validation, Supervision, Methodology, Investigation, Funding acquisition, Formal analysis, Conceptualization. **Martina Palomino-Schätzlein:** Writing – review & editing, Writing – original draft, Methodology, Investigation. **Laureano E. Carpio:** Writing – review & editing, Methodology, Investigation. **Camino de Juan Romero:** Writing – review & editing, Writing – original draft, Visualization, Validation, Supervision, Resources, Methodology, Investigation, Funding acquisition, Formal analysis, Conceptualization. **David Recio-Moreno:** Visualization, Methodology, Investigation, Formal analysis. **María Gabriela Álvarez-Rodríguez:** Methodology, Investigation, Formal analysis.

Declaration of Competing Interest

The authors declare that they have no known competing financial interests or personal relationships that could have appeared to influence the work reported in this paper.

Acknowledgements and funding

This research was funded by Instituto de Salud Carlos III (ISCIII) and cofounded by European Social Fund (ERDF/ESF, “Investing in your future”) [PI22/00824 to CdJ]; by Conselleria de Educación, Cultura, Universidades y Empleo (Comunidad Valenciana) [CIAICO 2024/0017 to CdJ and JLN]; and by HORIZON European Union [EXPLORA GA nº 101181841 to JLN]. The funders had no role in the study design, data collection and analysis, decision to publish, or preparation of the manuscript.

We thank Dr. Xisong Ke for providing the first commercial powder samples of SAA.

Appendix A. Supporting information

Supplementary data associated with this article can be found in the online version at doi:10.1016/j.biopha.2025.118935.

Data availability

Data will be made available on request. All the materials are available upon reasonable request from the corresponding authors.

References

[1] F. Bray, M. Laversanne, H. Sung, J. Ferlay, R.L. Siegel, I. Soerjomataram, A. Jemal, Global cancer statistics 2022: GLOBOCAN estimates of incidence and mortality worldwide for 36 cancers in 185 countries, CA Cancer J. Clin. 74 (2024) 229–263, https://doi.org/10.3322/CAAC.21834.

[2] M. Diefenhardt, D. Martin, R.-D. Hofheinz, M. Ghadimi, E. Fokas, C. Rödel, M. Fleischmann, Persistent lymph node metastases after neoadjuvant chemoradiotherapy for rectal cancer, JAMA Netw. Open 7 (2024) e2432927, https://doi.org/10.1001/JAMANETWORKOPEN.2024.32927.

[3] Y. Liu, C. Fang, J. Luo, C. Gong, L. Wang, S. Zhu, Traditional Chinese medicine for cancer treatment, Am. J. Chin. Med. 52 (2024) 583–604, https://doi.org/10.1142/S0192415X24500253.

[4] L. Zhou, Z. Zuo, M.S.S. Chow, Danshen: an overview of its chemistry, pharmacology, pharmacokinetics, and clinical use, J. Clin. Pharm. 45 (2005) 1345–1359, https://doi.org/10.1177/0091270005282630.

[5] J.A. Rothwell, V. Knaze, R. Zamora-Ros, Polyphenols: dietary assessment and role in the prevention of cancers, Curr. Opin. Clin. Nutr. Metab. Care 20 (2017) 512–521, https://doi.org/10.1097/MCO.0000000000000424.

[6] Y. Zhou, J. Zheng, Y. Li, D.P. Xu, S. Li, Y.M. Chen, H.Bin Li, Natural polyphenols for prevention and treatment of cancer, Nutrients 8 (2016), https://doi.org/10.3390/NU8080515.

[7] K.B. Pandey, S.I. Rizvi, Plant polyphenols as dietary antioxidants in human health and disease, Oxid. Med Cell Longev. 2 (2009) 270–278, https://doi.org/10.4161/OXIM.2.5.9498.

[8] S. Ma, D. Zhang, H. Lou, L. Sun, J. Ji, Evaluation of the anti-inflammatory activities of tanshinones isolated from Salvia miltiorrhiza var. Alba roots in THP-1 macrophages, J. Ethnopharmacol. 188 (2016) 193–199, https://doi.org/10.1016/j.jep.2016.05.018.

[9] C. Spatafora, C. Tringali, Natural-derived polyphenols as potential anticancer agents, Anticancer Agents Med Chem. 12 (2012) 902–918, https://doi.org/10.2174/187152012802649996.

[10] C.Y. Su, Q.L. Ming, K. Rahman, T. Han, L.P. Qin, Salvia miltiorrhiza: traditional medicinal uses, chemistry, and pharmacology, Chin. J. Nat. Med 13 (2015) 163–182, https://doi.org/10.1016/S1875-5364(15)30002-9.

[11] T. Qin, A. Rasul, A. Sarfraz, I. Sarfraz, G. Hussain, H. Anwar, A. Riaz, S. Liu, W. Wei, J. Li, X. Li, Salvianolic acid A & B: Potential cytotoxic polyphenols in battle against cancer via targeting multiple signaling pathways, Int J. Biol. Sci. 15 (2019) 2256–2264, https://doi.org/10.7150/IJBS.37467.

[12] A.E. Yuzhalin, Citrullination in cancer, Cancer Res 79 (2019) 1274–1284, https://doi.org/10.1158/0008-5472.CAN-18-2797/661345/P/CITRULLINATION-IN-CANCERCITRULLINATION-IN-CANCER.

[13] N.S. Gudmann, N.U.B. Hansen, A.C.B. Jensen, M.A. Karsdal, A.S. Siebuhr, Biological relevance of citrullinations: Diagnostic, prognostic and therapeutic options, Autoimmunity 48 (2015) 73–79, https://doi.org/10.3109/08916934.2014.962024.

[14] A. Ishigami, N. Maruyama, Importance of research on peptidylarginine deiminase and citrullinated proteins in age-related disease, Geriatr. Gerontol. Int 10 (2010) S53–S58, https://doi.org/10.1111/J.1447-0594.2010.00593.X.

[15] B. György, E. Tóth, E. Tarcsa, A. Falus, E.I. Buzás, Citrullination: A posttranslational modification in health and disease, Int J. Biochem Cell Biol. 38 (2006) 1662–1677, https://doi.org/10.1016/J.BIOCEL.2006.03.008.

[16] J.L. Neira, S. Araujo-Abad, A. Cámara-Artigas, B. Rizzuti, O. Abian, A.M. Giudici, A. Velazquez-Campoy, C. de Juan Romero, Biochemical and biophysical characterization of PADI4 supports its involvement in cancer, Arch. Biochem Biophys. 717 (2022) 109125, https://doi.org/10.1016/J.ABB.2022.109125.

[17] D.J. Slade, S. Horibata, S.A. Coonrod, P.R. Thompson, A novel role for protein arginine deiminase 4 in pluripotency: the emerging role of citrullinated histone H1 in cellular programming, BioEssays 36 (2014) 736–740, https://doi.org/10.1002/BIES.201400057;SUBPAGE:STRING:FULL.

[18] Y. Wang, R. Chen, Y. Gan, S. Ying, The roles of PAD2- and PAD4-mediated protein citrullination catalysis in cancers, Int J. Cancer 148 (2021) 267–276, https://doi.org/10.1002/IJC.33205.

[19] E. Witalison, P. Thompson, L. Hofseth, Protein Arginine Deiminases and Associated Citrullination: Physiological Functions and Diseases Associated with Dysregulation, Curr. Drug Targets 16 (2015) 700–710, https://doi.org/10.2174/1389450116666150202160954.

[20] C. Yang, Z.Z. Dong, J. Zhang, D. Teng, X. Luo, D. Li, Y. Zhou, Peptidylarginine deiminases 4 as a promising target in drug discovery, Eur. J. Med Chem. 226 (2021), https://doi.org/10.1016/j.ejmech.2021.113840.

[21] S. Ying, S. Dong, A. Kawada, T. Kojima, S. Chavanas, M.C. Méchin, V. Adoue, G. Serre, M. Simon, H. Takahara, Transcriptional regulation of peptidylarginine deiminase expression in human keratinocytes, J. Dermatol. Sci. 53 (2009) 2–9, https://doi.org/10.1016/J.JDERMSCI.2008.09.009.

[22] H.C. Hung, C.Y. Lin, Y.F. Liao, P.C. Hsu, G.J. Tsay, G.Y. Liu, The functional haplotype of peptidylarginine deiminase IV (S55G, A82V and A112G) associated with susceptibility to rheumatoid arthritis dominates apoptosis of acute T leukemia Jurkat cells, Apoptosis 12 (2007) 475–487, https://doi.org/10.1007/S10495-006-0005-0.

[23] M.T. Bertran, R. Walmsley, T. Cummings, I.V. Aramburu, D.J. Benton, R. Mora Molina, J. Assalaarachchi, M. Chasampalioti, T. Swanton, D. Joshi, S. Federico, H. Okkenhaug, L. Yu, D. Oxley, S. Walker, V. Papayannopoulos, H. Suga, M. A. Christophorou, L.J. Walport, A cyclic peptide toolkit reveals mechanistic principles of peptidylarginine deiminase IV regulation, Nat. Commun. 15 (2024) 9746, https://doi.org/10.1038/S41467-024-53554-1.

[24] C. Yang, Z.Z. Dong, J. Zhang, D. Teng, X. Luo, D. Li, Y. Zhou, Peptidylarginine deiminases 4 as a promising target in drug discovery, Eur. J. Med Chem. 226 (2021), https://doi.org/10.1016/J.EJMECH.2021.113840.

[25] P. Li, H. Yao, Z. Zhang, M. Li, Y. Luo, P.R. Thompson, D.S. Gilmour, Y. Wang, Regulation of p53 target gene expression by peptidylarginine deiminase 4, Mol. Cell Biol. 28 (2008) 4758, https://doi.org/10.1128/MCB.01747-07.

[26] P. Li, D. Wang, H. Yao, P. Doret, G. Hao, Q. Shen, H. Qiu, X. Zhang, Y. Wang, G. Chen, Y. Wang, Coordination of PAD4 and HDAC2 in the regulation of p53-

target gene expression, Oncogene 29 (2010) 3153–3162, https://doi.org/10.1038/onc.2010.51.
[27] J.L. Neira, B. Rizzuti, O. Abián, S. Araujo-Abad, A. Velázquez-Campoy, C. de Juan Romero, Human Enzyme PADI4 Binds to the Nuclear Carrier Importin α3, Cells 11 (2022) 2166, https://doi.org/10.3390/CELLS11142166/S1.
[28] J.L. Neira, B. Rizzuti, S. Araujo-Abad, O. Abian, M.E. Fárez-Vidal, A. Velazquez-Campoy, C. de Juan Romero, The armadillo-repeat domain of Plakophilin 1 binds to human enzyme PADI4, Biochim. Et. Biophys. Acta (BBA) Proteins Proteom. 1871 (2023) 140868, https://doi.org/10.1016/J.BBAPAP.2022.140868.
[29] S. Araujo-Abad, B. Rizzuti, A. Villamarin-Ortiz, D. Pantoja-Uceda, C.M. Moreno-Gonzalez, O. Abian, A. Velazquez-Campoy, J.L. Neira, C. de Juan Romero, New insights into cancer: MDM2 binds to the citrullinating enzyme PADI4, Protein Sci. 32 (2023) e4723, https://doi.org/10.1002/PRO.4723;CTYPE:STRING:JOURNAL.
[30] J.L. Neira, B. Rizzuti, M. Palomino-Schätzlein, V. Rejas, O. Abian, A. Velazquez-Campoy, Citrullination at the N-terminal region of MDM2 by the PADI4 enzyme, Protein Sci. 34 (2025), https://doi.org/10.1002/PRO.70033.
[31] S. Araujo-Abad, J.L. Neira, B. Rizzuti, P. García-Morales, C. de Juan Romero, P. Santofimia-Castaño, J. Iovanna, Intrinsically Disordered Chromatin Protein NUPR1 Binds to the Enzyme PADI4, J. Mol. Biol. 435 (2023) 168033, https://doi.org/10.1016/J.JMB.2023.168033.
[32] S. Araujo-Abad, M. Fuentes-Baile, B. Rizzuti, J.F. Bazán, A. Villamarin-Ortiz, M. Saceda, E. Fernández, M. Vidal, O. Abian, A. Velazquez-Campoy, C. de Juan Romero, J.L. Neira, The intrinsically disordered, epigenetic factor RYBP binds to the citrullinating enzyme PADI4 in cancer cells, Int J. Biol. Macromol. 246 (2023), https://doi.org/10.1016/j.ijbiomac.2023.125632.
[33] S. Araujo-Abad, B. Rizzuti, L. Soto-Conde, M. Vidal, O. Abian, A. Velazquez-Campoy, J.L. Neira, C. de Juan Romero, Citrullinating enzyme PADI4 and transcriptional repressor RING1B bind in cancer cells, Int J. Biol. Macromol. 274 (2024) 133163, https://doi.org/10.1016/J.IJBIOMAC.2024.133163.
[34] S. Araujo-Abad, B. García-Peñarrubia, A.M. Giudici, J.L. Neira, B. Rizzuti, C. de Juan Romero, J.A. Poveda, The Citrullinating Enzyme PADI4 Binds to Lipids: Identification of New Target Interactions for Cancer Therapy, J. Mol. Biol. 437 (2025), https://doi.org/10.1016/j.jmb.2025.169297.
[35] S.C. Gill, P.H. von Hippel, Calculation of protein extinction coefficients from amino acid sequence data, Anal. Biochem 182 (1989) 319–326, https://doi.org/10.1016/0003-2697(89)90602-7.
[36] A. Czypionka, O.R. De Los Paños, M.G. Mateu, F.N. Barrera, E. Hurtado-Gómez, J. Gómez, M. Vidal, J.L. Neira, The isolated C-terminal domain of ring 1B is a dimer made of stable, well-structured monomers, Biochemistry 46 (2007) 12764–12776, https://doi.org/10.1021/BI701343Q.
[37] B. Birdsall, R.W. King, M.R. Wheeler, C.A. Lewis, S.R. Goode, R.B. Dunlap, G.C. K. Roberts, Correction for light absorption in fluorescence studies of protein-ligand interactions, Anal. Biochem 132 (1983) 353–361, https://doi.org/10.1016/0003-2697(83)90020-9.
[38] C.A. Royer, S.F. Scarlata, Chapter 5 Fluorescence Approaches to Quantifying Biomolecular Interactions, Methods Enzym. 450 (2008) 79–106, https://doi.org/10.1016/S0076-6879(08)03405-8.
[39] D. Beckett, Measurement and analysis of equilibrium binding titrations, A Begin. 'S. Guide Methods Enzym. 488 (2011) 1–16, https://doi.org/10.1016/B978-0-12-381268-1.00001-X.
[40] J.L. Neira, S. Vega, S. Martínez-Rodríguez, A. Velázquez-Campoy, The isolated GTPase-activating-protein-related domain of neurofibromin-1 has a low conformational stability in solution, Arch. Biochem Biophys. 700 (2021) 108767, https://doi.org/10.1016/J.ABB.2021.108767.
[41] J. Cavanagh, W.J. Fairbrother, A.G. Palmer, N.J. Skelton, Protein NMR Spectroscopy: principles and practice (2nd Edition), 2007.
[42] R. Huang, I.K.H. Leung, Protein–Small Molecule Interactions by WaterLOGSY, Methods Enzym. 615 (2019) 477–500, https://doi.org/10.1016/BS.MIE.2018.08.020.
[43] C. Dalvit, G.P. Fogliatto, A. Stewart, M. Veronesi, B. Stockman, WaterLOGSY as a method for primary NMR screening: Practical aspects and range of applicability, J. Biomol. NMR 21 (2001) 349–359, https://doi.org/10.1023/A:1013302231549.
[44] C. Dalvit, P. Pevarello, M. Tato, M. Veronesi, A. Vulpetti, M. Sundström, Identification of compounds with binding affinity to proteins via magnetization transfer from bulk water, J. Biomol. NMR 18 (2000) 65–68, https://doi.org/10.1023/A:1008354229396.
[45] M. Piotto, V. Saudek, V. Sklenář, Gradient-tailored excitation for single-quantum NMR spectroscopy of aqueous solutions, J. Biomol. NMR 2 (1992) 661–665, https://doi.org/10.1007/BF02192855.
[46] G. Bodenhausen, D.J. Ruben, Natural abundance nitrogen-15 NMR by enhanced heteronuclear spectroscopy, Chem. Phys. Lett. 69 (1980) 185–189, https://doi.org/10.1016/0009-2614(80)80041-8.
[47] M. Knipp, M. Vašák, A colorimetric 96-well microtiter plate assay for the determination of enzymatically formed citrulline, Anal. Biochem 286 (2000) 257–264, https://doi.org/10.1006/abio.2000.4805.
[48] P.L. Kearney, M. Bhatia, N.G. Jones, L. Yuan, M.C. Glascock, K.L. Catchings, M. Yamada, P.R. Thompson, Kinetic characterization of protein arginine deiminase 4: A transcriptional corepressor implicated in the onset and progression of rheumatoid arthritis, Biochemistry 44 (2005) 10570–10582, https://doi.org/10.1021/BI050292M.
[49] K. Sugawara, Y. Yoshizawa, S. Tzeng, W.L. Epstein, K. Fukuyama, Colorimetric determination of citrulline residues in proteins, Anal. Biochem 265 (1998) 92–96, https://doi.org/10.1006/ABIO.1998.2925.
[50] K. Ozvoldik, T. Stockner, E. Krieger, YASARA Model-Interactive Molecular Modeling from Two Dimensions to Virtual Realities, J. Chem. Inf. Model 63 (2023) 6177–6182, https://doi.org/10.1021/acs.jcim.3c01136.
[51] E. Krieger, G. Vriend, YASARA View - molecular graphics for all devices - from smartphones to workstations, Bioinformatics 30 (2014) 2981–2982, https://doi.org/10.1093/BIOINFORMATICS/BTU426.
[52] O. Trott, A.J. Olson, AutoDock Vina: Improving the speed and accuracy of docking with a new scoring function, efficient optimization, and multithreading, J. Comput. Chem. 31 (2010) 455–461, https://doi.org/10.1002/JCC.21334.
[53] N. Horikoshi, H. Tachiwana, K. Saito, A. Osakabe, M. Sato, M. Yamada, S. Akashi, Y. Nishimura, W. Kagawa, H. Kurumizaka, Structural and biochemical analyses of the human PAD4 variant encoded by a functional haplotype gene, Acta Crystallogr D. Biol. Crystallogr 67 (2011) 112–118, https://doi.org/10.1107/S0907444910051711.
[54] C.R. Harris, K.J. Millman, S.J. van der Walt, R. Gommers, P. Virtanen, D. Cournapeau, E. Wieser, J. Taylor, S. Berg, N.J. Smith, R. Kern, M. Picus, S. Hoyer, M.H. van Kerkwijk, M. Brett, A. Haldane, J.F. del Río, M. Wiebe, P. Peterson, P. Gérard-Marchant, K. Sheppard, T. Reddy, W. Weckesser, H. Abbasi, C. Gohlke, T.E. Oliphant, Array programming with NumPy, Nature 585 (2020) 357–362, https://doi.org/10.1038/S41586-020-2649-2.
[55] P. Virtanen, R. Gommers, T.E. Oliphant, M. Haberland, T. Reddy, D. Cournapeau, E. Burovski, P. Peterson, W. Weckesser, J. Bright, S.J. van der Walt, M. Brett, J. Wilson, K.J. Millman, N. Mayorov, A.R.J. Nelson, E. Jones, R. Kern, E. Larson, C. J. Carey, İ. Polat, Y. Feng, E.W. Moore, J. VanderPlas, D. Laxalde, J. Perktold, R. Cimrman, I. Henriksen, E.A. Quintero, C.R. Harris, A.M. Archibald, A.H. Ribeiro, F. Pedregosa, P. van Mulbregt, A. Vijaykumar, A. Pietro Bardelli, A. Rothberg, A. Hilboll, A. Kloeckner, A. Scopatz, A. Lee, A. Rokem, C.N. Woods, C. Fulton, C. Masson, C. Häggström, C. Fitzgerald, D.A. Nicholson, D.R. Hagen, D. V. Pasechnik, E. Olivetti, E. Martin, E. Wieser, F. Silva, F. Lenders, F. Wilhelm, G. Young, G.A. Price, G.L. Ingold, G.E. Allen, G.R. Lee, H. Audren, I. Probst, J. P. Dietrich, J. Silterra, J.T. Webber, J. Slavič, J. Nothman, J. Buchner, J. Kulick, J. L. Schönberger, J.V. de Miranda Cardoso, J. Reimer, J. Harrington, J.L. C. Rodríguez, J. Nunez-Iglesias, J. Kuczynski, K. Tritz, M. Thoma, M. Newville, M. Kümmerer, M. Bolingbroke, M. Tartre, M. Pak, N.J. Smith, N. Nowaczyk, N. Shebanov, O. Pavlyk, P.A. Brodtkorb, P. Lee, R.T. McGibbon, R. Feldbauer, S. Lewis, S. Tygier, S. Sievert, S. Vigna, S. Peterson, S. More, T. Pudlik, T. Oshima, T.J. Pingel, T.P. Robitaille, T. Spura, T.R. Jones, T. Cera, T. Leslie, T. Zito, T. Krauss, U. Upadhyay, Y.O. Halchenko, Y. Vázquez-Baeza, SciPy 1.0: fundamental algorithms for scientific computing in Python, Nat. Methods 17 (2020) 261–272, https://doi.org/10.1038/S41592-019-0686-2.
[56] N. Michaud-Agrawal, E.J. Denning, T.B. Woolf, O. Beckstein, MDAnalysis: A toolkit for the analysis of molecular dynamics simulations, J. Comput. Chem. 32 (2011) 2319–2327, https://doi.org/10.1002/JCC.21787;SUBPAGE:STRING:FULL.
[57] R.J. Gowers, M. Linke, J. Barnoud, T.J.E. Reddy, M.N. Melo, S.L. Seyler, J. Domański, D.L. Dotson, S. Buchoux, I.M. Kenney, O. Beckstein, MDAnalysis: A Python Package for the Rapid Analysis of Molecular Dynamics Simulations, Scipy (2016) 98–105, https://doi.org/10.25080/MAJORA-629E541A-00E.
[58] C. Bouysset, S. Fiorucci, ProLIF: a library to encode molecular interactions as fingerprints, J. Chemin.. 13 (2021) 1–9, https://doi.org/10.1186/S13321-021-00548-6/FIGURES/4.
[59] J. Ribeiro, C. Ríos-Vera, F. Melo, A. Schüller, Calculation of accurate interatomic contact surface areas for the quantitative analysis of non-bonded molecular interactions, Bioinformatics 35 (2019) 3499–3501, https://doi.org/10.1093/BIOINFORMATICS/BTZ062.
[60] M.P. Ventero, M. Fuentes-Baile, C. Quereda, E. Perez-Valeciano, C. Alenda, P. Garcia-Morales, D. Esposito, P. Dorado, V.M. Barbera, M. Saceda, Radiotherapy resistance acquisition in glioblastoma. Role of SOCS1 and SOCS3, PLoS One 14 (2019), https://doi.org/10.1371/JOURNAL.PONE.0212581.
[61] M. Fuentes-Baile, D. Bello-Gil, E. Pérez-Valenciano, J.M. Sanz, P. García-Morales, B. Maestro, M.P. Ventero, C. Alenda, V.M. Barberá, M. Saceda, CLyta-DAAO, free and immobilized in magnetic nanoparticles, induces cell death in human cancer cells, Biomolecules 10 (2020), https://doi.org/10.3390/BIOM10020222.
[62] Y.L. Liu, Y.H. Chiang, G.Y. Liu, H.C. Hung, Functional role of dimerization of human peptidylarginine deiminase 4 (PAD4), PLoS One 6 (2011), https://doi.org/10.1371/JOURNAL.PONE.0021314.
[63] J.E. Jones, C.P. Causey, B. Knuckley, J.L. Slack-Noyes, P.R. Thompson, Protein arginine deiminase 4 (PAD4): current understanding and future therapeutic potential, Curr. Opin. Drug Discov. Devel 12 (2009) 616. ⟨https://pmc.ncbi.nlm.nih.gov/articles/PMC3771078/⟩ (accessed May 16, 2025).
[64] T. Ye, R. Chen, Y. Zhou, J. Zhang, Z. Zhang, H. Wei, Y. Xu, Y. Wang, Y. Zhang, Salvianolic acid A (Sal A) suppresses malignant progression of glioma and enhances temozolomide (TMZ) sensitivity via repressing transgelin-2 (TAGLN2) mediated phosphatidylinositol-3-kinase (PI3K) / protein kinase B (Akt) pathway, Bioengineered 13 (2022) 11646–11655, https://doi.org/10.1080/21655979.2022.2070963.
[65] X. Zheng, S. Chen, Q. Yang, J. Cai, W. Zhang, H. You, J. Xing, Y. Dong, Salvianolic acid A reverses the paclitaxel resistance and inhibits the migration and invasion abilities of human breast cancer cells by inactivating transgelin 2, Cancer Biol. Ther. 16 (2015) 1407–1414, https://doi.org/10.1080/15384047.2015.1070990.
[66] C.X. Li, Q. Xu, S.T. Jiang, D. Liu, C. Tang, W.L. Yang, Anticancer effects of salvianolic acid A through multiple signaling pathways (Review), Mol. Med. Rep. 32 (2025), https://doi.org/10.3892/MMR.2025.13541.
[67] Y. Yang, L. Zhang, X. La, Z. Li, H. Li, S. Guo, Salvianolic acid A inhibits tumor-associated angiogenesis by blocking GRP78 secretion, Naunyn Schmiede Arch. Pharm. 392 (2019) 467–480, https://doi.org/10.1007/S00210-018-1585-2.
[68] L. Bonaccini, A. Karioti, M.C. Bergonzi, A.R. Bilia, Effects of Salvia miltiorrhiza on CNS Neuronal Injury and Degeneration: A Plausible Complementary Role of Tanshinones and Depsides, Planta Med 81 (2015) 1003–1016, https://doi.org/10.1055/S-0035-1546196.

[69] W. Zhong, B. Sun, W. Gao, Y. Qin, H. Zhang, L. Huai, Y. Tang, Y. Liang, L. He, X. Zhang, H. Tao, S. Chen, W. Yang, L. Yang, Y. Liu, H. Liu, H. Zhou, T. Sun, C. Yang, Salvianolic acid A targeting the transgelin-actin complex to enhance vasoconstriction, EBioMedicine 37 (2018) 246–258, https://doi.org/10.1016/j.ebiom.2018.10.041.

[70] W.Y. Wu, Y.P. Wang, Pharmacological actions and therapeutic applications of Salvia miltiorrhiza depside salt and its active components, Acta Pharm. Sin. 33 (2012) 1119–1130, https://doi.org/10.1038/APS.2012.126.

[71] J.H.C. Ho, C.Y. Hong, Salvianolic acids: Small compounds with multiple mechanisms for cardiovascular protection, J. Biomed. Sci. 18 (2011), https://doi.org/10.1186/1423-0127-18-30.

[72] M. Zheng, Y. Zhang, Y. Xu, Y. Han, Y. Wu, J. Kang, Chemoproteomics and phosphoproteomics profiling reveals salvianolic acid a as a covalent inhibitor of mTORC1, J. Proteome Res 22 (2023) 2450–2459, https://doi.org/10.1021/ACS.JPROTEOME.3C00188/ASSET/IMAGES/LARGE/PR3C00188_0006.JPEG.

[73] A. Karioti, F. Carta, C.T. Supuran, Phenols and polyphenols as carbonic anhydrase inhibitors, Vol. 21, Page 1649, Molecules 2016 21 (2016) 1649, https://doi.org/10.3390/MOLECULES21121649.

[74] B. Jiang, D. Li, Y. Deng, F. Teng, J. Chen, S. Xue, X. Kong, C. Luo, X. Shen, H. Jiang, F. Xu, W. Yang, J. Yin, Y. Wang, H. Chen, W. Wu, X. Liu, D. an Guo, Salvianolic Acid A, a novel matrix metalloproteinase-9 inhibitor, prevents cardiac remodeling in spontaneously hypertensive rats, PLoS One 8 (2013), https://doi.org/10.1371/JOURNAL.PONE.0059621.

[75] J. Cai, S. Chen, W. Zhang, X. Zheng, S. Hu, C. Pang, J. Lu, J. Xing, Y. Dong, Salvianolic acid A reverses paclitaxel resistance in human breast cancer MCF-7 cells via targeting the expression of transgelin 2 and attenuating PI3 K/Akt pathway, Phytomedicine 21 (2014) 1725–1732, https://doi.org/10.1016/j.phymed.2014.08.007.

[76] Y.L. Liu, I.C. Tsai, C.W. Chang, Y.F. Liao, G.Y. Liu, H.C. Hung, Functional roles of the non-catalytic calcium-binding sites in the N-terminal domain of human peptidylarginine deiminase 4, PLoS One 8 (2013), https://doi.org/10.1371/JOURNAL.PONE.0051660.

[77] G.Y. Liu, Y.L. Liu, C.Y. Lee, Y.N. Huang, H.Y. Chen, H.C. Hung, Probing the Roles of Calcium-Binding Sites during the Folding of Human Peptidylarginine Deiminase, Sci. Rep. 7 (2017) 1–14, https://doi.org/10.1038/S41598-017-02677-1;TECHMETA=80,82,83,9;SUBJMETA=2272,2273,45,470,57,631;KWRD=MOLECULAR+CONFORMATION,PROTEIN+FOLDING.

[78] K. Arita, H. Hashimoto, T. Shimizu, K. Nakashima, M. Yamada, M. Sato, Structural basis for Ca2+-induced activation of human PAD4, Nat. Struct. Mol. Biol. 11 (2004) 777–783, https://doi.org/10.1038/NSMB799.

[79] X. Zhou, S. Kong, A. Maker, S.G. Remesh, K.K. Leung, K.A. Verba, J.A. Wells, Antibody discovery identifies regulatory mechanisms of protein arginine deiminase 4, Nat. Chem. Biol. 20 (2024) 742–750, https://doi.org/10.1038/S41589-023-01535-8.

[80] X. Zhang, M. Shen, H. Zhu, J. Zhang, M. Yang, K. Su, Y. Zhang, W. Fu, X. Ke, Y. Qu, Small molecule activates citrullination through targeting PAD2, Philos. Trans. R. Soc. B Biol. Sci. 378 (2023), https://doi.org/10.1098/RSTB.2022.0248.

[81] L.J. Byrnes, W.Y. Choi, P. Balbo, M.E. Banker, J. Chang, S. Chen, X. Cheng, Y. Cong, J. Culp, H. Di, M. Griffor, J. Hall, X. Meng, B. Morgan, J.J. Mousseau, J. Nicki, T. O'Connell, S. Ramsey, A. Shaginian, S. Shanker, J. Trujillo, J. Wan, F. Vincent, S. W. Wright, F. Vajdos, Discovery, characterization, and structure of a cell active PAD2 inhibitor acting through a novel allosteric mechanism, ACS Chem. Biol. 19 (2024), https://doi.org/10.1021/ACSCHEMBIO.4C00397.